NAVAL POSTGRADUATE SCHOOL
Monterey, California

THESIS

CONTINUOUS MEASUREMENT OF AGING RESPONSE
IN ALUMINUM ALLOYS BY EDDY CURRENT METHODS

by

Silvester Galvan Mata

December 1993

Thesis Advisor: Terry R. McNelley

Approved for public release; distribution is unlimited.

REPORT DOCUMENTATION PAGE

Form Approved OMB No. 0704

1. AGENCY USE ONLY	2. REPORT DATE 17 December 1993	3. REPORT TYPE AND DATES COVERED Master's Thesis

4. TITLE AND SUBTITLE: CONTINUOUS MEASUREMENTS OF AGING RESPONSE IN ALUMINUM ALLOYS BY EDDY CURRENT METHODS

5. FUNDING NUMBERS

6. AUTHOR(S) *Mata, Silvester Galvan*

7. PERFORMING ORGANIZATION NAME(S) AND ADDRESS(ES)
Naval Postgraduate School
Monterey, CA 93943-5000

8. PERFORMING ORGANIZATION REPORT NUMBER

9. SPONSORING/MONITORING AGENCY NAME(S) AND ADDRESS(ES)

10. SPONSORING/MONITORING AGENCY REPORT NUMBER

11. SUPPLEMENTARY NOTES The views expressed in this thesis are those of the author and do not reflect the official policy or position of the Department of Defense or the U.S. Government.

12a. DISTRIBUTION/AVAILABILITY STATEMENT
Approved for public release; distribution is unlimited.

12b. DISTRIBUTION CODE
*A

13. ABSTRACT
The objective of this research was to investigate further the use of a sensor system to continuously monitor the aging response of heat treatable aluminum alloys. This concept of continuous monitoring is referred to as "Intelligent Processing". The bridge consists of eddy current coils incorporated in an impedance bridge circuit, with modifications following earlier work by Esarey. The system continuously monitors a material property, resistivity, indicative of the aging process. The results of such continuous measurements, combined with mechanical test data, will allow one to gain active control of the aging process and hence the material properties of aluminum alloys. The ultimate results would be higher reliability of engineering structures. The increased precision in control of heat treatment processes would allow more narrow performance and greater service life of engineering structures.

14. SUBJECT TERMS
Aging response, Continuous measurement, Aluminum alloys, Eddy current methods

15. NUMBER OF PAGES 71

16. PRICE CODE

17. SECURITY CLASSIFICATION OF REPORT	18. SECURITY CLASSIFICATION OF THIS PAGE	19. SECURITY CLASSIFICATION OF ABSTRACT	20. LIMITATION OF ABSTRACT
Unclassified	Unclassified	Unclassified	UL

NSN 7540-01-280-5500

Standard Form 298 (Rev. 2-89)
Prescribed by ANSI STD. 239-18

Approved for public release; distribution is unlimited.

Continuous Measurement of Aging Response in
Aluminum Alloys by *Eddy Current Methods*

by

Silvester G. Mata
Lieutenant, United States Navy
B.S., U.S. Naval Academy, 1985

Submitted in partial fulfillment
of the requirements for the degree of

MASTER OF SCIENCE IN MECHANICAL ENGINEERING

from the

NAVAL POSTGRADUATE SCHOOL
December 1993

Author: Silvester G Mata
Silvester Galvan Mata

Approved by: T R McNelley
Terry R. McNelley, Thesis Advisor

Matthew Kelleher
Matthew D. Kelleher, Chairman
Department of Mechanical Engineering

ABSTRACT

The objective of this research was to investigate further the use of a sensor system to continuously monitor the aging response of heat treatable aluminum alloys. This concept of continuous monitoring is referred to as "Intelligent Processing". The sensor consists of eddy current coils incorporated in an impedance bridge circuit, with modifications following earlier work by Esarey. The system continuously monitors a material property, resistivity, indicative of the aging process. The results of such continuous measurements, combined with mechanical test data, will allow one to gain active control of the aging process and hence the material properties of aluminum alloys. The ultimate results would be higher reliability of engineering structures. The increased precision in control of heat treatment processes would allow more narrow performance and greater service life of engineering structures.

TABLE OF CONTENTS

ACKNOWLEDGEMENT

A special thanks to my thesis advisor, Professor Terry McNelley, for allowing me to take on this project in the area of intelligent processing.

The endless technological support received from Tom Christian, Jim Schofield, Doug Shelton and the Naval Postgraduate School machine shop, who often responded with "eleventh hour" assistance which was greatly appreciated.

The Naval Air Warfare Center, and especially the support of Dr. William Frazier, Program Monitor, in the continuing development of the the intelligent processing concept. Their help and support is much acknowledged and appreciated.

To my family, the most important people in my life, thanks for all the love, understanding and support, especially to my wife, Leslie. Finally, to my rosebud of a daughter, Emily, who unknowingly made my day with her smile.

I. INTRODUCTION

The primary goal of this research was to improve a sensor system designed and developed by Esarey [Ref. 1]. The device was intended to be used to continuously monitor, in real time, the isothermal age hardening response of Aluminum alloys. The sensor would continuously monitor the evolution of a material property, resistivity, which is indicative of the progress of the heat treatment process. This would allow the heat treatment to be terminated when the desired physical and mechanical properties have been achieved rather than at an arbitrary time. This concept of process monitoring is called *"Intelligent Processing"*. The results of such a continuous measurement combined with mechanical test data will allow one to gain active control of the aging process and hence the material properties of aluminum alloys. The ultimate result would be higher reliability of engineering structures. The increased precision in control of heat treatment processes would allow more narrow specification and ultimately result in higher performance and greater service life of engineering structures. With this goal in mind, Esarey [Ref. 1] initially investigated the possibility of utilizing existing eddy current resistivity measuring equipment in combination with a computerized system to "intelligently" monitor the progress of the aging process of aluminum alloys.

Eddy current measuring devices currently exist. However, they provide a measurement of a material's resistivity only at standard temperature conditions as part of a post-heat treatment evaluation. Such devices give results in absolute values of resistivity ($\mu\Omega$*mm) or relative values based on the International Annealed Copper Standard (IACS). In this system, the conductivity of fully annealed, unalloyed copper is arbitrarily rated at 100%, and the conductivities of other metals and alloys are expressed as some percentage of this standard. Thus, the conductivity of an unalloyed aluminum is rated 61% IACS, or 61% that of unalloyed copper. The resistivities and conductivities of several common metals and alloys are give in Table 1.1. [Ref. 2]

The age hardening of heat-treatable Aluminum alloys essentially consists of a three-step process. First, the alloy is solutionized at a temperature within the single phase solid solution region of the phase diagram. Next, the material is quickly cooled to room temperature which is within a two-phase region. This quenching step prevents any diffusion and accompanying formation of the second phase. During the third stage, i.e. the aging process, the supersaturated single-phase solid is heated to a temperature below the solvus for the alloy in question. Now, precipitation of the solute occurs and some form of a second-phase dispersion is allowed to develop. Heat treatment schedules have been developed by a trial and error to

correspond to desired mechanical, electrical, corrosion and other properties. The practice of applying such heat treatment schedules in a "cookbook" fashion does not allow real-time evaluation of the progress of the age hardening process. Thus, no adjustments of control parameters can be made during aging and destructive and non-destructive tests, used only after the heat treatment process is complete, allow determination of whether the heat treatment was success or failure.

Esarey [Ref. 1] developed a monitoring technique based on the fact that sensing relative resistivity changes during aging rather than measuring absolute resistivity values was all that was needed to accurately reflect the progress of the aging process. The system consisted of the following components:

1) Two spiral-wound sensor probes mounted in a testing frame;
2) A bridge carrier/amplifier which included an oscillator, impedance bridge circuit, demodulator, and signal amplifier/filter;
3) A Hewlett Packard 3478A Digital Multimeter;
4) And an IBM compatible PC (with a DT2801 series data acquisition board to collect time and voltage data for subsequent use).

Utilizing the above equipment, time and impedance bridge unbalance (r.m.s.) voltage data files were obtained. Plots of aging time versus voltage were generated. Mechanical evaluation which included Rockwell hardness, yield strength,

ultimate yield stress and percentage elongation, were performed at the T6 temper aging temperature of 120° C. Plots of aging time versus hardness, yield strength, ultimate yield strength, and percent elongation were generated. The plots revealed an initial increase in resistivity to a maximum, followed by a decrease in resistivity. More importantly, the rate of increase and decrease in resistivity increased as the aging temperature became higher, reflecting the increased rate of precipitation at higher aging temperature.

The following chapters will develop further the background on this subject and then present the modifications to improve this apparatus for this work. Further results will be described and mechanical property data will be provided for correlation with the resistivity measurements.

Table 1.1 RESISTIVITIES AND CONDUCTIVITIES OF SEVERAL COMMON METALS AND ALLOYS (Adapted from Metals Handbook, v.17, American Society for metals, 1991, p.168)

Metal or alloy	Resistivity μΩ•mm	Conductivity % IACS
Silver	16.3	105
Copper, annealed	17.2	100
Gold	24.4	70
Aluminum	28.8	61
Aluminum alloys		
6061-T6	41	42
7075-T6	53	32
2024-T4	52	30
Magnesium	46	37
70-30 Brass	62	28
Phosphor Bronzes	160	11
Monel	482	3.6
Zirconium	500	3.4
Zircaloy-2	720	2.4
Titanium	548	3.1
Ti-6Al-4V alloy	1720	1.0
Type 304 stainless steel	700	2.5
Inconel 600	980	1.7
Hastelloy X	1150	1.5
Waspaloy	1230	1.4

II. BACKGROUND

A. Electrical Resistivity

The sensor system of interest in this research relies on resistance to induced eddy currents to evaluate the extent of heat treatment for a material. In order to understand how an eddy currents relate to the resistivity of the aluminum alloy samples, it is necessary to have a basic knowledge of resistivity. Simply stated, resistivity is a measure of a material's resistance to the passage of an electric current. When an electric field is applied, current flow, or movement of free electrons, results from the biasing of the motion of these electrons. A simple picture regards free electrons as moving randomly through the lattice. If the lattice were perfect, motion, at least in some directions, would encounter little impediment. Interaction with the lattice will result from crystal lattice imperfections which cause scattering, i.e., collisions of moving electrons and rebound from such defects. This scattering phenomenon may be described by several parameters including electron drift velocity, v_d, and mobility, μ_e, which are related to the applied electric field, ξ, as follows:

$$\mu_e = \frac{v_d}{\xi} \qquad 2.1$$

The resistivity, ρ, of a material is given by the relation

$$\rho = \frac{1}{\mu_e n q} \qquad 2.2$$

where μ_e is the mobility, q is the charge on each electron (1.6×10^{-19} C), and n is the number of electrons. Therefore, electrical resistivity is proportional to both the number of free electrons and the electron mobility. A schematic diagram showing the path of an electron that is deflected by scattering events is shown in Figure 2.1. Also shown is drift velocity. Essentially, as the frequency of scattering collision with lattice defects increases, the drift velocity decreases. Thus, mobility is lowered and correspondingly the resistivity is increased. The electron mobility of pure aluminum is 13.04 $cm^2/V*sec$. [Ref. 3]

B. Effects of Temperature, Lattice Defects and Plastic Deformations on Resistivity

It has been observed the total resistivity of a metal is the linear sum of the contributions from thermal vibrations, ρ_t, lattice defects, ρ_d, and plastic deformation, ρ_d, that is

$$\rho = \rho_t + \rho_d + \rho_p \qquad (2.3)$$

Equation 2.3 is commonly known as **Matthiessen's Rule**. [Ref. 2]

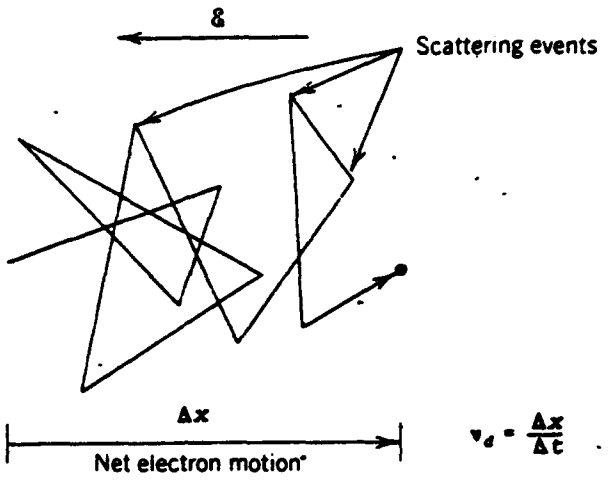

Figure 2.1 Schematic Diagram Showing the Path of an Electron that is Deflected by Scattering Events. Also Shown is Drift Velocity. (Mostly from William D. Callister, Jr., Materials Science and Engineering, An Introduction, John Wilely & Sons, Inc., New York, 1985)

1. Thermal Effects

Resistivity increases with temperature as shown in Figure 2.2(a)and (b). The thermal resistivity component is due to the increase in amplitude of thermal vibrations as temperature increases, resulting in more effective electron scattering. For pure metals at intermediate temperatures, the resistivity rises linearly with temperature as shown in Figure 2.3. Thus, the temperature dependence of resistivity is given by

$$\rho = \rho_0 + aT \qquad (2.4)$$

where ρ_0 and a are constants for a particular metal or alloy.

2. Changes Due to Lattice Defects

Various lattice imperfections may also scatter electrons and thus reduce the mean free path between collisions. For this reason mobility is reduced and resistivity is thereby increased. Scattering defects include solute impurities, vacancies, dislocations and interfacial defects. The separate effects of these defects are independent of each other and of temperature as shown in Figure 2.2(c). [Ref. 3]

3. Changes Due to Plastic Deformation

Plastic deformation increases the dislocation density. Dislocations also scatter electrons and thus increasing the number of dislocations also raises the resistivity. The effect of deformation on resistivity is also illustrated in Figure 2.3.

4. Combined Effects of Temperature and Lattice Defects

The total resistivity due to the contributions of temperature and lattice defects (and neglecting contributions due to plastic deformation) is given by the equation:

$$\rho_{Total} = \rho_T + \rho_d \qquad (2.5)$$

The primary objective of this research is to obtain a measure of the change in an alloy's resistivity as a function of the change in defect resistivity, ρ_d, during isothermal aging. The change in the defect contribution to resistivity

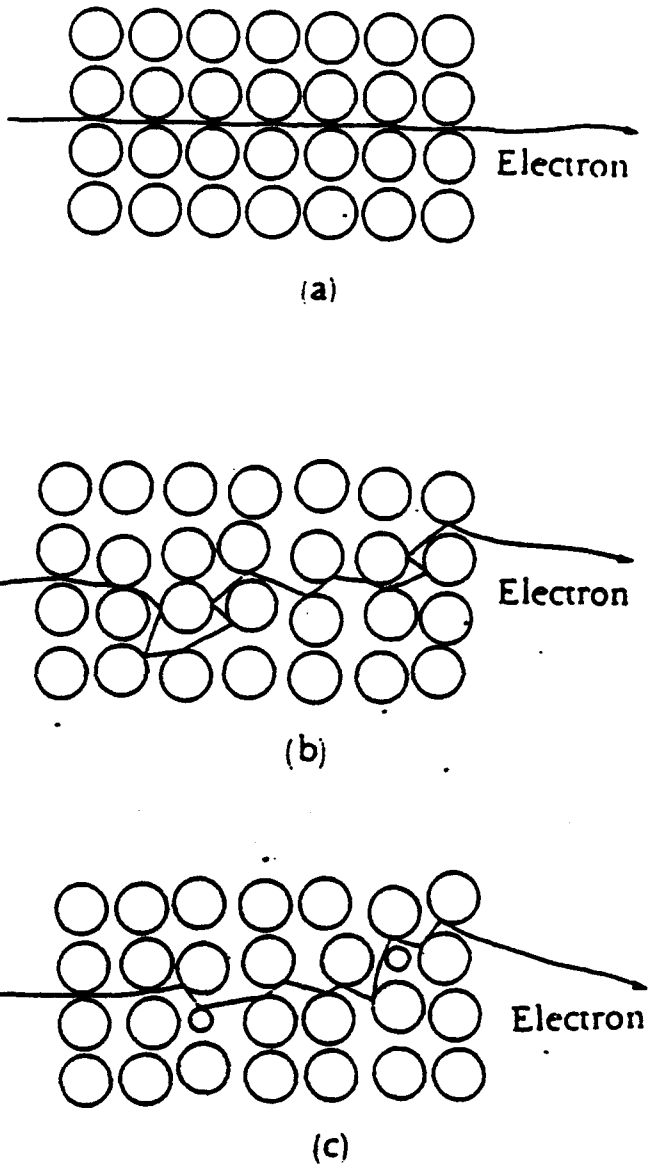

Figure 2.2 Movement of an Electron Through (a) Perfect Crystal, (b) Crystal Heated to a High Temperature, (c) Crystal Containing Lattice Defects. (Taken from D.R. Askeland, Science and Engineering of Materials, PWS-KENT, Boston, 1984)

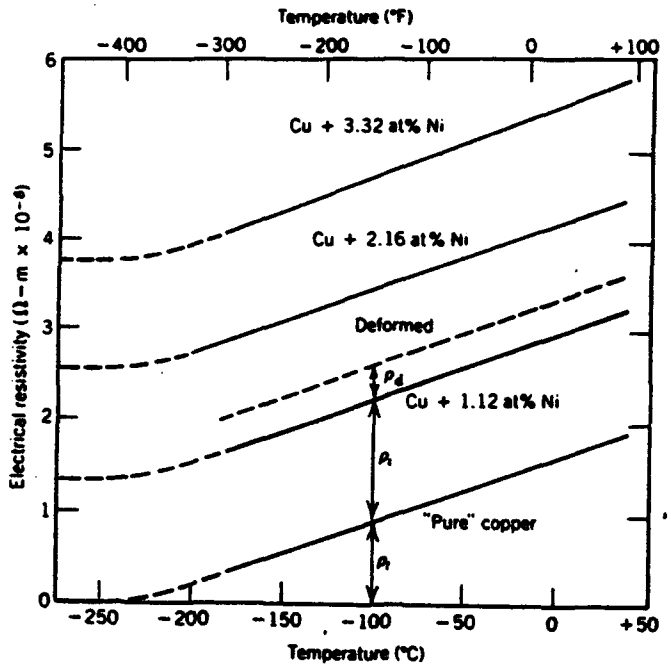

Figure 2.3 Schematic Representation of the Temperature Dependence of Copper and Various Copper-Nickel Alloys. Deformation Contributions are Indicated at -100^{0}C. (Adapted from J.O. Linde, Ann. Physik, 5, 219 (1932); and C.A. Wert and R.M. Thomson, Physics of Solids, 2nd edition, McGraw-Hill Book Company, New York, 1970; and D.R. Callister, Material Science and Engineering, An Introduction, 2nd edition, John Wiley & Sons, Inc., New York, 1985)

during decomposition of a supersaturated condition reflects the change in charge carrier mean free path during precipitation. As the precipitation process occurs, the charge-carrier mean free path becomes greater as solute atoms are removed from solution. This would result in the being resistivity lowered. If large strain fields are developed in the initial stages of precipitation (i.e. GP zone formation), resistivity may increase initially before decreasing later

since such lattice strains will also scatter electrons in much the same manner as dislocation strain fields.

C. Eddy Current Testing

1. Eddy Current Theory

Eddy current techniques have been used for many years to inspect electrically conductive materials for defects, irregularities in structure, and to evaluate such characteristics such as hardness and condition of heat-treatment. Discussion will be limited to the measurement of resistivity as it is affected by hardening heat treatments. Further details of eddy current theory are given in References *2 and 5-10.*

When a coil carrying an alternating current is brought near a sample of conductive material to be tested, a magnetic field is generated within the coil which induces an electric current the test sample. Typically, the pattern of the induced currents resemble the eddies in flowing streams of turbulent water and therefore they are called eddy currents. The generation of the eddy currents is shown in Figure 2.4. The magnitude of the eddy currents depends on the magnitude and frequency of the alternating current. The material factors affecting the magnitude of the induced eddy currents are the resistivity and magnetic permeability of the test specimen (See earlier discussion of resistivity located in this

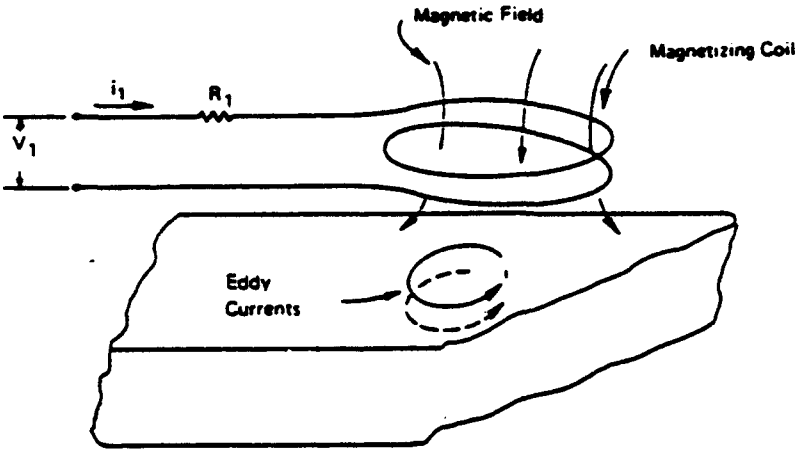

Figure 2.4 Eddy Current Generation Schematic. (Taken from National Aeronautics and Space Administration Report 5113 (NASA SP-5113), Non-destructive Testing: A Survey, p.102, 1973)

chapter). Age-hardenable aluminum alloys such as Al 7075 are paramagnetic and have magnetic permeabilities very close to 1.0. Furthermore, the magnetic permeability is unaffected by processing and heat treatment. The induced eddy currents set up a magnetic field which opposes the original magnetic field and varies the apparent impedance of the coil. Therefore, the change in the alloy's resistivity, as affected temperature and various lattice defects, is the variable exploited in this work. Since changes in lattice defects correspond to changes in mechanical properties, the monitoring of resistivity changes can provide an indicator of changing mechanical properties during age hardening.[6-10]

2. Other Operating Variables

Several other system variables encountered during eddy current measurements are described below.

a. Skin Effect

When alternating fields are present eddy currents are not distributed evenly throughout the sample but instead are concentrated near the surface of the material. The depth at which the magnitude of the eddy currents is reduced exponentially to approximately 37% of the surface value is referred to as the skin depth. This depth of penetration is given by

$$\delta = \sqrt{\frac{\rho}{f\mu_o\sigma}} \qquad 2.6$$

where δ = depth of penetration (meters);

f = frequency (hertz);

μ = magnetic permeability ($4\pi \times 10^{-7}$ henry/meters for non-magnetic materials), and

ρ = electrical resistivity (ohms*meters)

A standard chart for depths of penetration is shown in Figure 2.5.

b. Lift-Off Factor

The magnitude of induced eddy currents in a conductor depends on the distance between the source of the field, i.e. the coil, and the surface of the material being

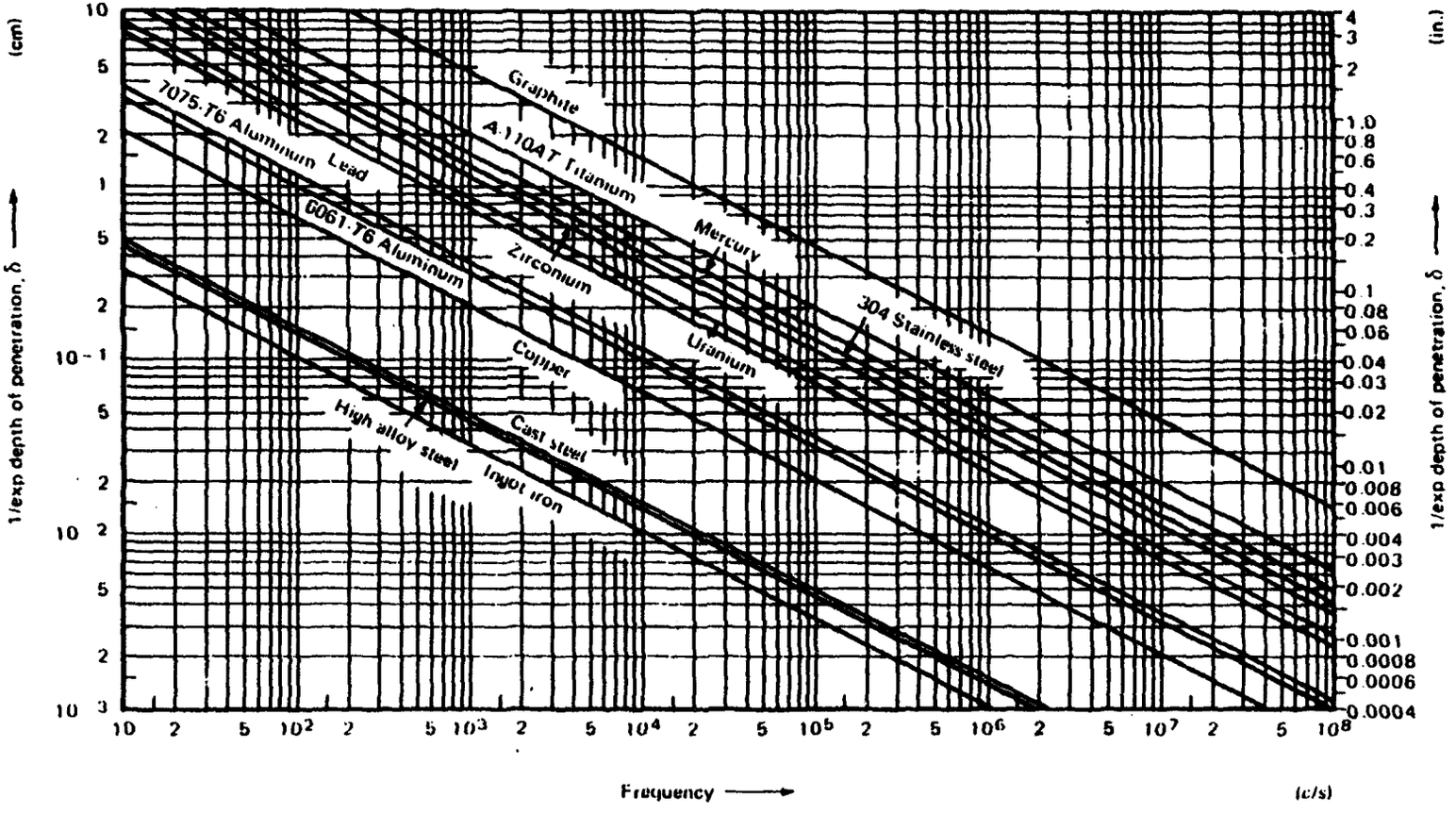

Figure 2.5 Skin depth for frequencies between 10 Hz and 10^8 Hz inplane conductors of various materials. (Courtesy of The Macmillan Company, Richard Hochschild; Microwave Instruments Co. and National Aeronautical Space Administration)

examined. This dependence is referred to as the ***"lift-off" effect***. For high frequencies, testing may be so sensitive to lift-off that small variations can mask many indications from the conditions of primary interest. Therefore, it is necessary to maintain a constant relationship between the size and shape of the coils and samples.

c. Edge Effect

When the eddy-current coil approaches the end or edge of a sample, the eddy currents are distorted because they are unable to flow beyond the edge of the sample. This distortion of the eddy current is known as ***"edge effect"***.

D. Precipitation in Age-Hardenable Alloys

An understanding of the factors governing the precipitation process in age-hardenable aluminum alloys is necessary to understand fully how the heat treatment affects the desired mechanical properties of age-hardenable aluminum alloys. Further details of precipitation processes in age-hardenable aluminum alloys are presented in References 11 through 15. Aluminum-copper alloys have been extensively studied and will be used to illustrate the essential ideas.

1. Precipitation in Aluminum-Copper Alloys

Figure 2.6 shows the decreasing solubility required for precipitation-hardening in an alloy system. As briefly discussed in the previous chapter, an aluminum alloy is first

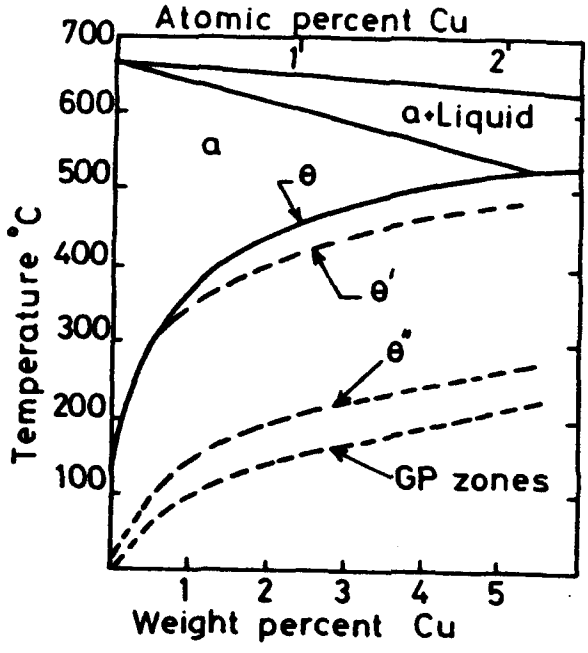

Figure 2.6 Al-Rich Al-Cu Binary Diagram Sshowing GP, θ", θ', and Solvus Lines. (Reproduced from G. Lorimer, Precipitation Processes in Solids, K.C. Russel and H.I. Aaronson (Eds.), The Metallurgical Society of AMIE, 1978, p. 87 and D.A. Porter and K.E. Easterling, Phase Transformations in Metals and Alloys, Van Nostrand, Rheinhold (UK), 1987, p. 291)

heated to a temperature within the single α phase (Al) region and then quickly quenched to room temperature. The rapid cooling suppresses the separation of the θ-phase so that the alloy exists at the lower temperature in a metastable supersaturated condition. The next stage, the aging heat treatment, is the most critical because it is here that the precipitation temperature and the duration of heating at the

specified temperature have the greatest effect on the mechanical and physical properties.

In a supersaturated Al-Cu alloy, there is a driving force for precipitation of the equilibrium θ phase, $CuAl_2$. If the alloy is aged at a temperature between room temperature and about 100^0 C, the first form of the precipitate to nucleate is the coherent, Cu-rich, Guinier-Preston (GP1) zones. With the passage of time, these transform to GP2, then to θ'' and finally to the equilibrium θ. At temperatures between 100^0 C and 180^0C, the GP1 zones do not appear and the GP2 zones appear initially. These sequence are illustrated in the C-curves at the right of Figure 2.7. That GP zones nucleate before the stable, incoherent θ phase can be explained on the basis of relative activation barriers. The GP zones are coherent with the matrix and thus a have low activation energy barrier for formation, whereas the θ phase is incoherent and has a higher activation energy barrier. The shape of the precipitates also varies. The strain energy due to formation of the coherent GP1 Zones is minimized when the zones are disc-shaped. On the other hand, equilibrium θ-phase particles tend to adopt a spheroidal shape to minimize interfacial energy.

Figure 2.8 illustrates how hardness is increased by adjusting the precipitation heat treatment temperature. The as-quenched hardness is low since solid solution strengthening due to Cu in solution is limited. The increase in hardness

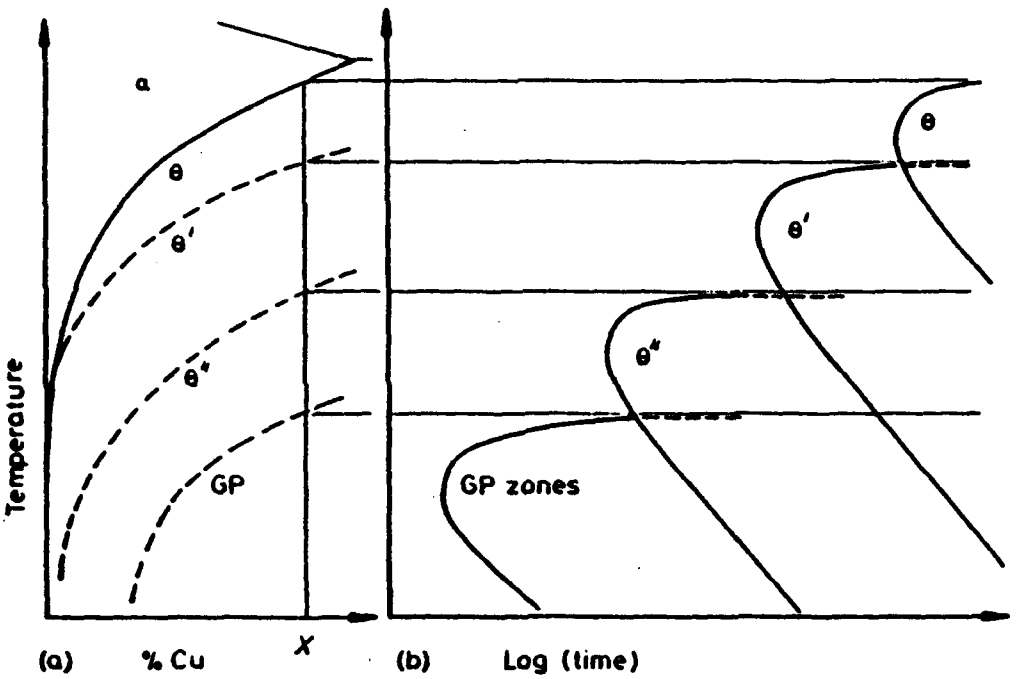

Figure 2.7 (a) Metastable Solvus Line in Al-Cu (schematic) (b) Time for Start of Precipitation at Different Temperatures for Alloy X in (a). (Taken from D.A. Porter, K.E. Easterling, Phase Transformations in Metals and Alloys, Van Nostrand Reinhold, 1987, p.291)

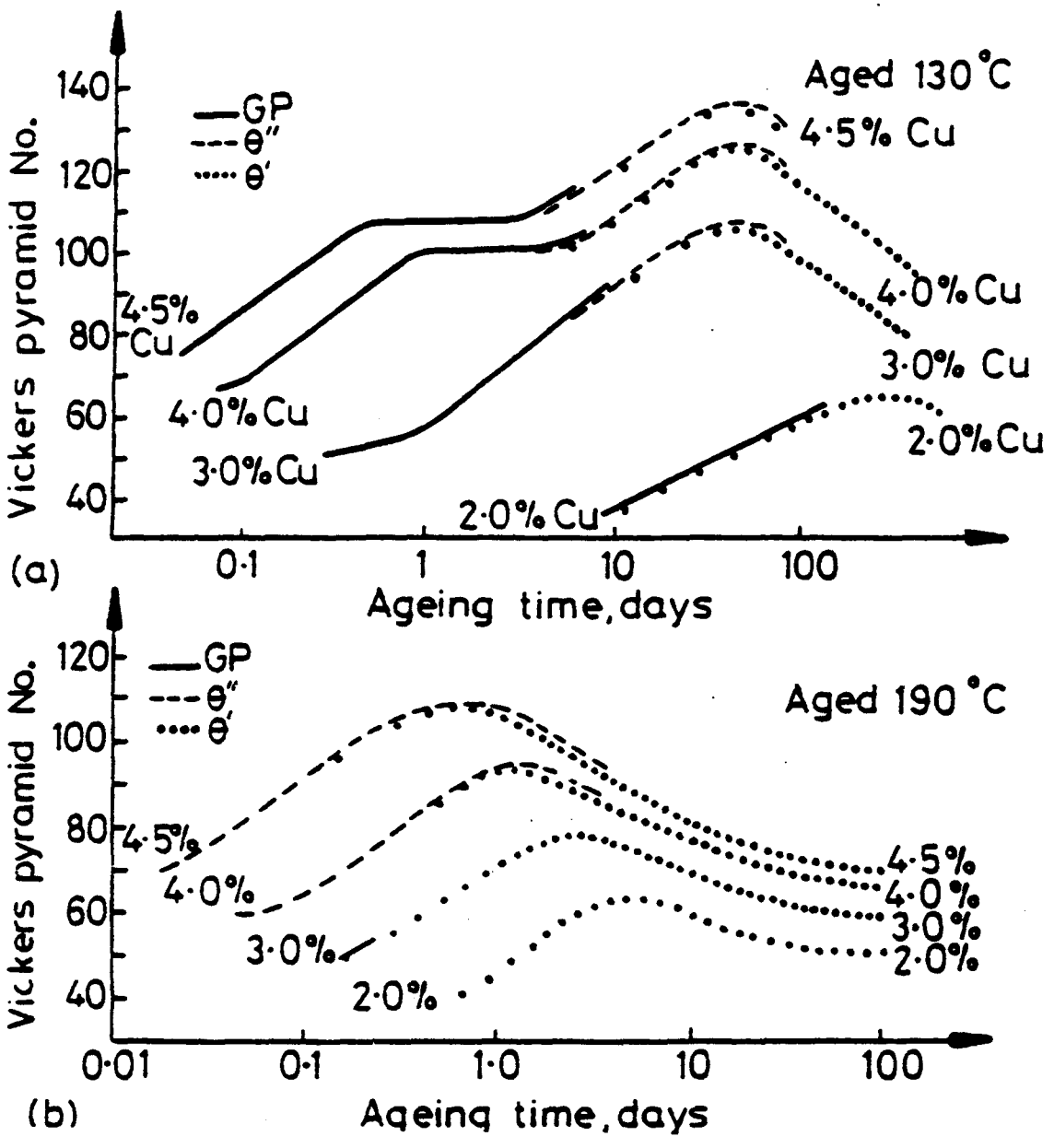

Figure 2.8 Hardness vs Time for Various Al-Cu Alloys at (a) 130°C (b) 190°C. (After J.M. Silcock, T.J. Heal and H.K. Hardy, Journal of the Institute of Metals 82 (1953-1954) 239 and D.A. Porter and K.E. Easterling, Phase Transformations in Metals and Alloys, Van Nostrand Reinhold,1987, p.307)

immediately after the aging commences is caused by the resistance to dislocation movement provided by the strain fields of the GP zones. The hardness continues to increase with the formation of GP2 or θ'' zones because the dislocations are forced through a highly strained matrix. Eventually, the spacing between precipitates becomes so large that dislocations are able to bow between the precipitates and hardness begins to decrease. Further aging will coarsen the precipitates and also decrease hardness. This condition is called overaging and should be avoided. [Ref. 11]

2. Precipitation in Aluminum-Zinc-Magnesium (Al-Zn-Mg) Alloys

The aging process in Al-Zn-Mg alloys results in spherically shaped GP zones. With increased time, the GP zones grow and thus the strength of the alloy increases. The GP zones pass through a transition form known as η' or **M'**, the precursor of the equilibrium $MgZn_2$, η, or **M** phase precipitate. The basal planes of the hexagonal η' precipitates are partially coherent with the {111} matrix planes but the interface between the c-direction of the precipitate is incoherent relative to the matrix. It is this incoherency that gives the alloys its increased strength. [Ref.13] The standard aging sequence for Al-Zn-Mg is

SS → GP zones (spherical) → M' → M

where the equilibrium phase, M, is $MgZn_2$.

Several studies have demonstrated that the actual aging sequence varies with a slight change in composition. A list of possible phases formed in Al-Zn-Mg alloys is given in Table 2.1. For example one possible aging sequence is

SS → GP zones (spherical) → T′ → T

where T is Mg_3Zn_3Al. Figure 2.9 illustrates the different phases present in Al-Zn-Mg alloys.

The formation of intermediate phases and the respective properties of an alloy with 6.5% Zn and 2.5% Mg are illustrated in Figures 10 and 11.

Table 2.1 PROBABLE PHASES FORM IN AL-ZN-MG ALLOYS (Taken from Moldolfo, L.F., *Aluminum Alloys, Structures and Properties*, Butterworths, 1976, p. 585)

Mg	< 1% Mg in solid soln.	Zn:Mg ≪ 1 Mg_3Al_8	Zn:Mg = 1–2 $Mg_3Zn_3Al_2$	Zn:Mg > 2.2 $MgZn_2$	with Si Mg_2Si	Cu > Mg $CuMgAl_2$	Cr > Mg $Cr_2Mg_3Al_{18}$	Mn > Mg $(MgMn)_3Al_{10}$
Zn	< 3% Zn in solid soln.	> 3% Zn Zn:Mg < 2.2 $Mg_3Zn_3Al_2$	> 3% Zn Zn:Mg > 2 $MgZn_2$	Mn > Zn Mn_3ZnAl_{24}				
Cu	< 1% Cu in solid soln.	> 1% Cu in soln. in $MgZn_2$ or $Mg_3Zn_3Al_2$	Cu > Mg $CuMgAl_2$	Cu ≫ Mg $CuAl_2$	Fe > Cu Cu_2FeAl_7	Fe + Mn > 1.5% $(CuFeMn)Al_6$	Mn > 1% Fe < 0.2% $Cu_2Mn_3Al_{20}$	
Fe	Fe ≫ Si $FeAl_3$	Fe < 3 Si Fe_2SiAl_8	Si < Fe Mn > 1/2 Fe $(FeMn)Al_6$	Si < Fe Cr > 1/2 Fe $(FeCr)Al_7$	Si > Fe Mn > 1/2 Fe $(FeMn)_3Si_2Al_{15}$	Si > Fe Cr > 1/2 Fe $(CrFe)_4Si_4Al_{13}$	Fe > Cu Si, Mn, Cr < 1/5 Fe Cu_2FeAl_7	
Si	Mg_2Si	Zn > 5%, Si > 3 Fe Mg > 3 Zn Fe_2SiAl_8	Si > Fe, Mg < 3 Zn Mn > 1/2 Fe $(FeMn)_3Si_2Al_{15}$		Si > Fe, Mg < 3 Zn Cr > 1/2 Fe $(CrFe)_4Si_4Al_{13}$			
Mn	Si ≪ Mn $(FeMn)Al_6$	Si ≪ Mn Mn > Cu, Fe < Mn $Cu_2Mn_3Al_{20}$	Si > Mn Zn > 5% $(FeMn)_3Si_2Al_{15}$	Cr = Mn Fe < Mn $(CrMn)Al_{12}$	Mn > Mg Zn < 2 Mg $(MgMn)_3Al_{10}$	Mn > Zn Mn_3ZnAl_{24}		
Cr	Si < Cr $(CrFe)Al_7$	Mn = Cr, Fe < Mn $(CrMn)Al_{12}$						
Zr	No Cr, Mn $ZrAl_3$	Mn > Zr in soln. in $MnAl_6$	Cr > Zr in soln. in $CrAl_7$					

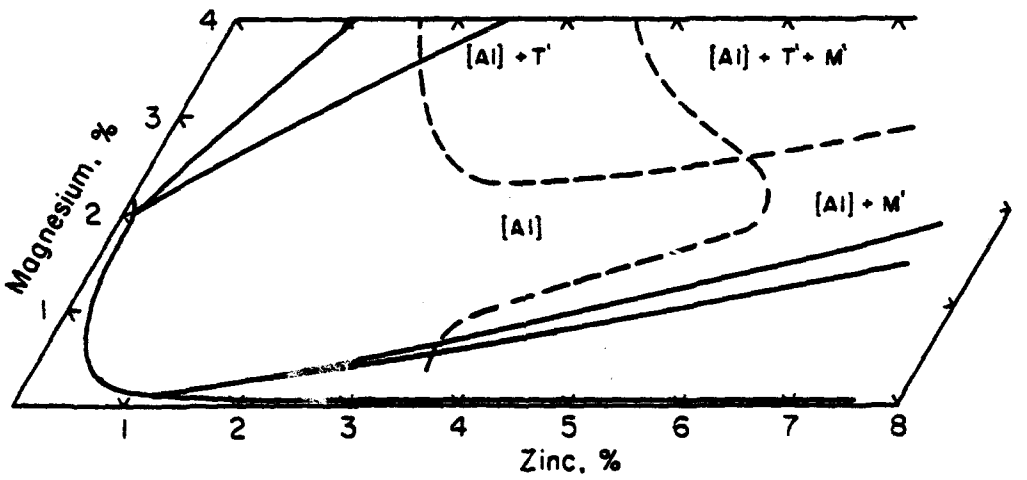

Figure 2.9 Comparison of Phases Present in Al-Zn-Mg Alloys. Fields Separated by Dashed Lines Identify Phases Present After Alloys Were Solution Heat Treated, Quenched, and Aged 24 h at 120^{0}C ([Al]=GP zone structure). Fields Separated by Solid Lines are Phases in Equilibrium at 175^{0}C.(H.C. Stumpf, Alcoa and John E. Hatch, Aluminum, Properties and Physical Metallurgy, American Society for Metals, 1984)

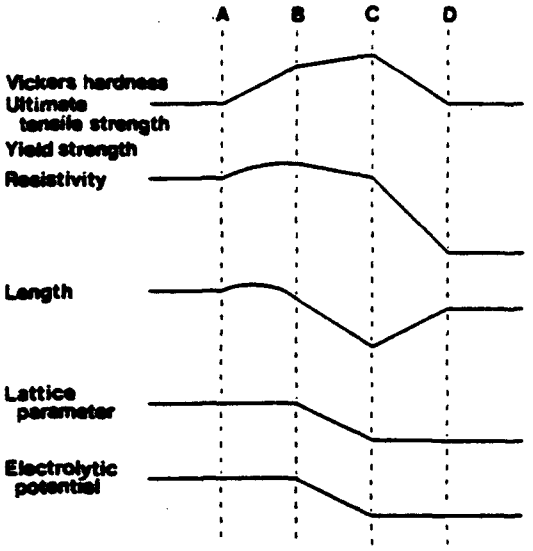

Figure 2.10 Schematic Plot of Changes in Properties During Aging of an Alloy with 6.5% Zn, 2.5%Mg. (Taken from Moldolfo, L.F., *Aluminum Alloys, Structures and Properties*, Butterworths, 1976, p. 585)

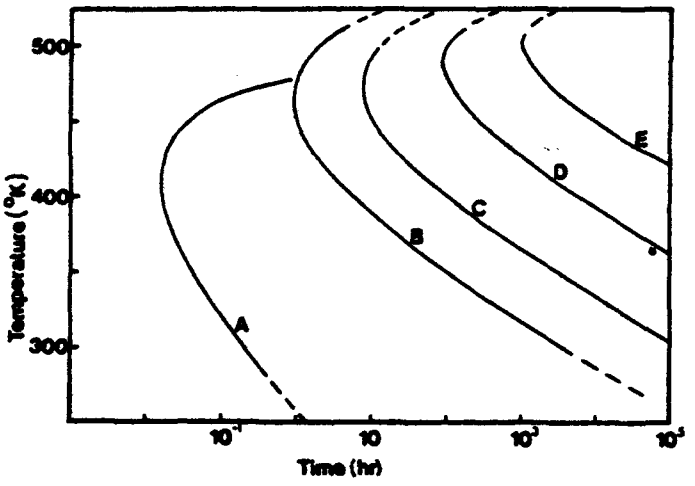

Figure 2.11 TTT Curves for an Alloy with 6.5%Zn, 2.5%Mg. (Taken from Moldolfo, L.F., *Aluminum Alloys, Structures and Properties*, Butterworths, 1976, p. 585)

E. Initial Sensor Design and Evaluation

Esarey[1] initiated this effort to design, fabricate and test a simple eddy current sensor device incorporating a impedance bridge circuit which could be used to monitor in real-time the isothermal age-hardening of aluminum alloys. With modifications, such a device may also be useful in monitoring aging processes in other material as well.

The sensor system was devised based on the premise that sensing relative resistivity changes during aging versus obtaining absolute resistivity values would accurately reflect the aging process. Esarey was able to reach this goal as illustrated in Figure 2.12. These data from Esarey's work illustrate the change in bridge imbalance voltage with time for aging at various temperatures. The initial increase reflects a transient as temperature equilibrates. The subsequent decrease reflects the decreasing resistivity of the alloy as precipitation occurs. Note the increased rate of aging at higher aging temperatures.

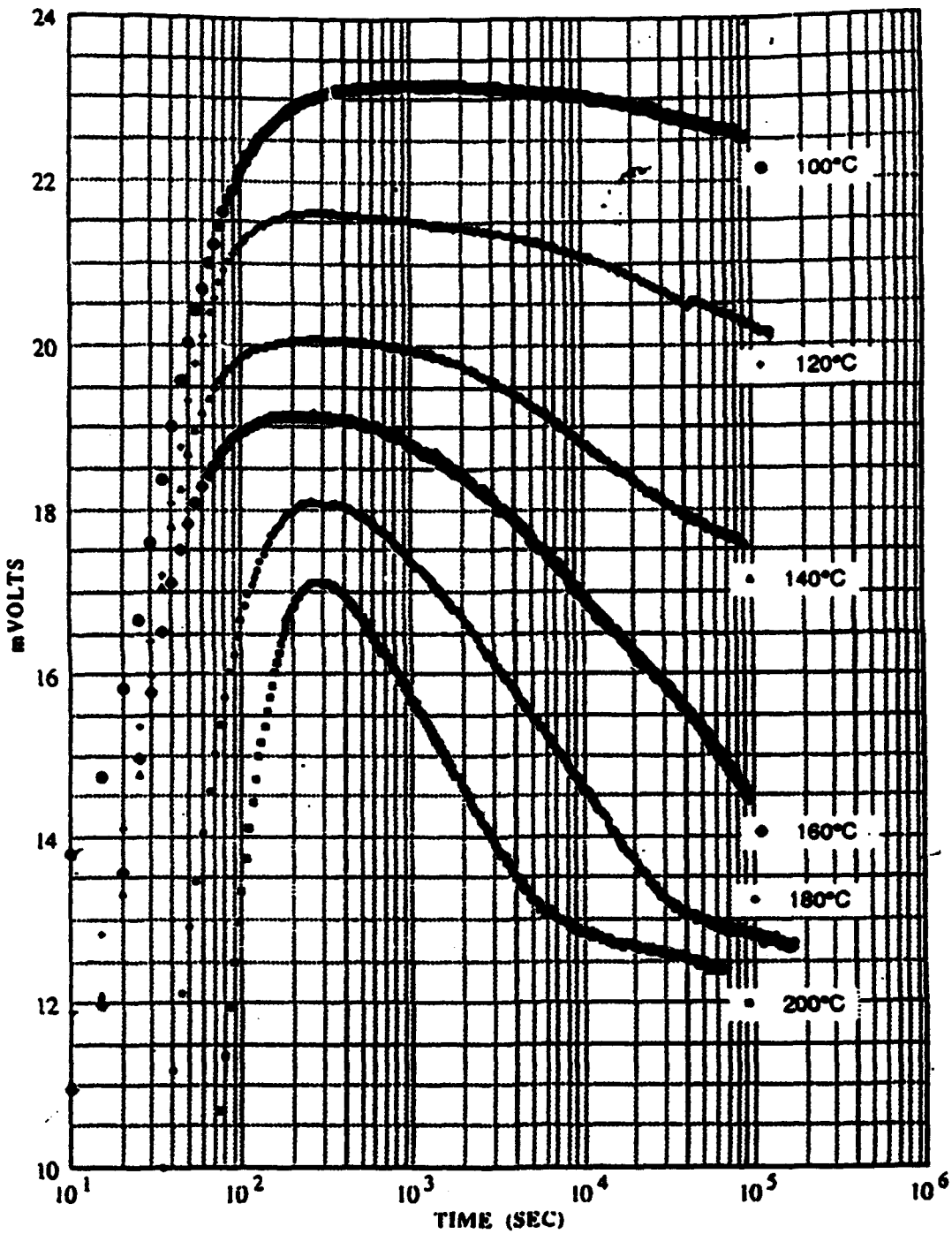

Figure 2.12 Experimental Bridge Output Response for Al 7075 Aged at Various Temperatures taken by Esarey.

III. EXPERIMENTAL PROCEDURES AND COMPONENT DESIGN

A. Initial Sensor System and Modifications

The apparatus designed by Esarey is shown in the schematic of Figure 3.1. A shortcoming of this system was that the bridge output was in RMS voltage values. This made the initial "nulling" process difficult and hence a residual voltage value had to be subtracted from the final output voltage data reflecting the inability to achieve a zero null. A second problem was that the probe and sample positioning could vary and improved repeatability of positioning was required.

Several modifications were made to the sensor system which include:

(1) The impedance bridge circuit was incorporated in a Bridge Carrier Amplifier/Filter (B.C.A.). The B.C.A. synchronously demodulated the bridge output signal. The nulling process now allows measurement from above the nominal element resistant through zero to below the nominal element reactance value.

(2) The probe coils within the testing apparatus were inverted to provide more consistent probe and sample positioning.

The final sensor system configuration is shown in Figure 3.2.

B. Experimental Procedures

The step-by-step procedure for use of the modified system is listed below:

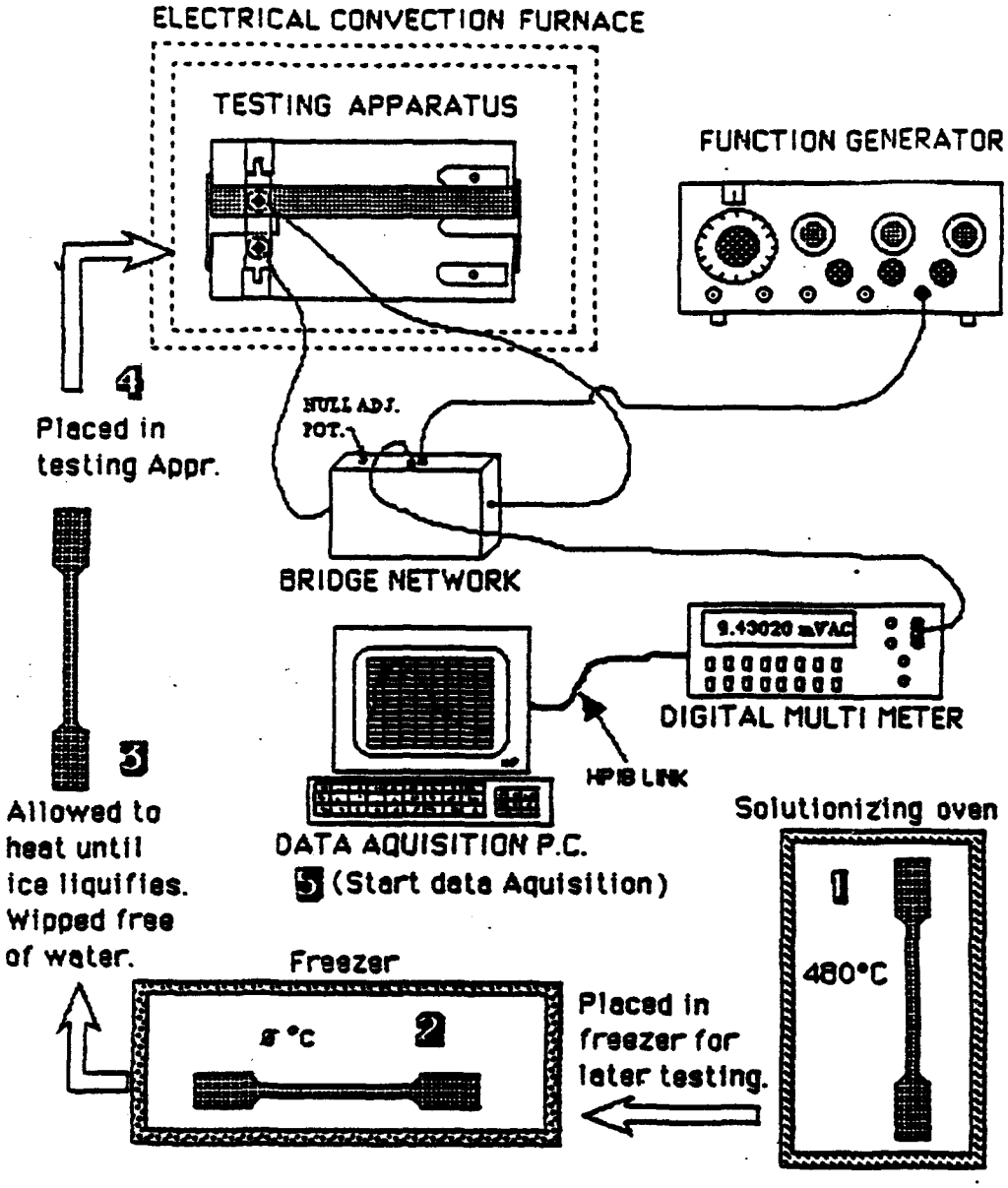

Figure 3.1 Initial Testing System and Processing Schematic Diagram.

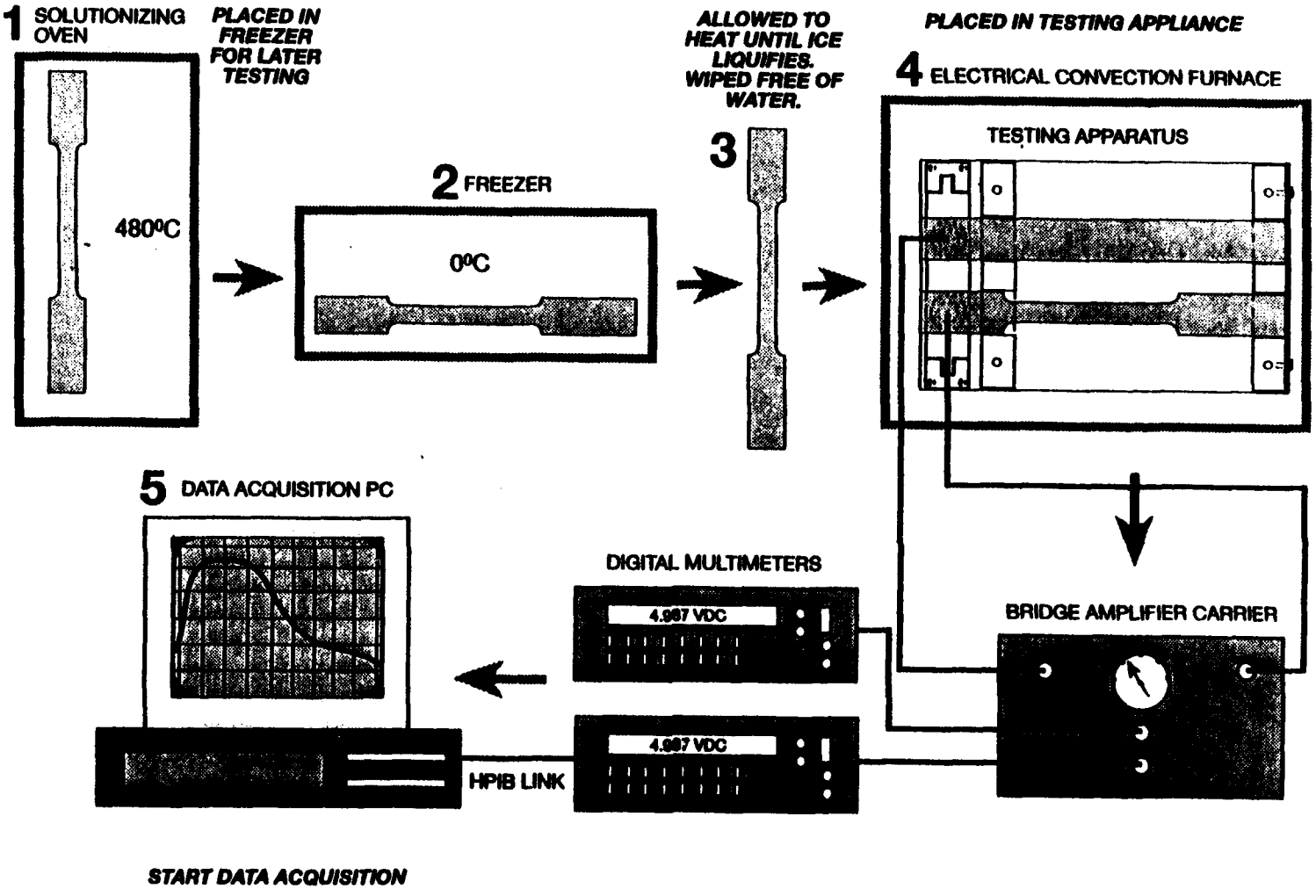

Figure 3.2 Final Testing System and Processing Schematic Diagram.

(1) Al 7075 tensile samples were solutionized at approximately 480°C for 50 minutes.

(2) Samples were quickly quenched in a large water bath at approximately 25°C.

(3) All samples were immediately placed in cold storage at approximately -15°C.

(4) The convection furnace was set at the desired aging temperature with the testing apparatus inside and pure aluminum test sample resting on each probe.

(5) With isothermal furnace conditions verified and all system component settings and circuit connections verified, the data acquisition program was given the desired instructions regarding timing of sampling intervals for measuring the bridge unbalance voltage (output voltage)

(6) A sample was removed from cold storage and allowed to warm until moisture could be removed from sample.

(7) Upon opening the furnace, the pure aluminum sample was removed and the alloy sample inserted over the testing probe(right probe) and the furnace was closed as quickly as possible.

(8) The data acquisition program was started, generating time versus voltage data files based on instructions given in step 5.

(9) The samples were immediately quenched at the conclusion of aging and stored in cold storage for further mechanical testing.

(10) The samples were removed from cold storage for hardness and tensile testing.

C. Component design changes

The following paragraphs describe the major changes were made to the testing apparatus and electrical circuitry to improve the repeatability of monitoring process.

1. Testing Apparatus Design

The probe coils were inverted within the redesigned testing apparatus. Now samples rest on top of the probes and this improves the consistency of probe and sample positioning. The testing apparatus is shown in Figures 3.3 and 3.4. Probe coils are shown separately as illustrated in Figure 3.5.

2. Bridge Carrier Amplifier/Filter (B.C.A.)

A block diagram of the B.C.A. is shown in Figure 3.6. It provides a means of detecting changes in resistivity a test sample by measuring the change of inductive reactance between the eddy current coils of the impedance bridge circuit. The B.C.A. consists of an oscillator, instrumentation amplifier, phase sensitive demodulator and amplifier/filter. The oscillator is set at 5 volts RMS and 52 Khz based on test probe type and dimensions. Field changes to the oscillator can be made but are not recommended. The excitation signal is next amplified by a 500 gain instrumentation amplifier.

The amplified signal acts as an input signal to the bridge circuit. A simplified bridge circuit is drawn in Figure 3.7. The bridge output is then synchronously demodulated in attempt to make the "nulling" process much more accurate and to make easier the location the "null" voltage. The signal is next amplified and filtered to an output range of +/-10 volts direct current (dc) for maximum usefulness and clarity.

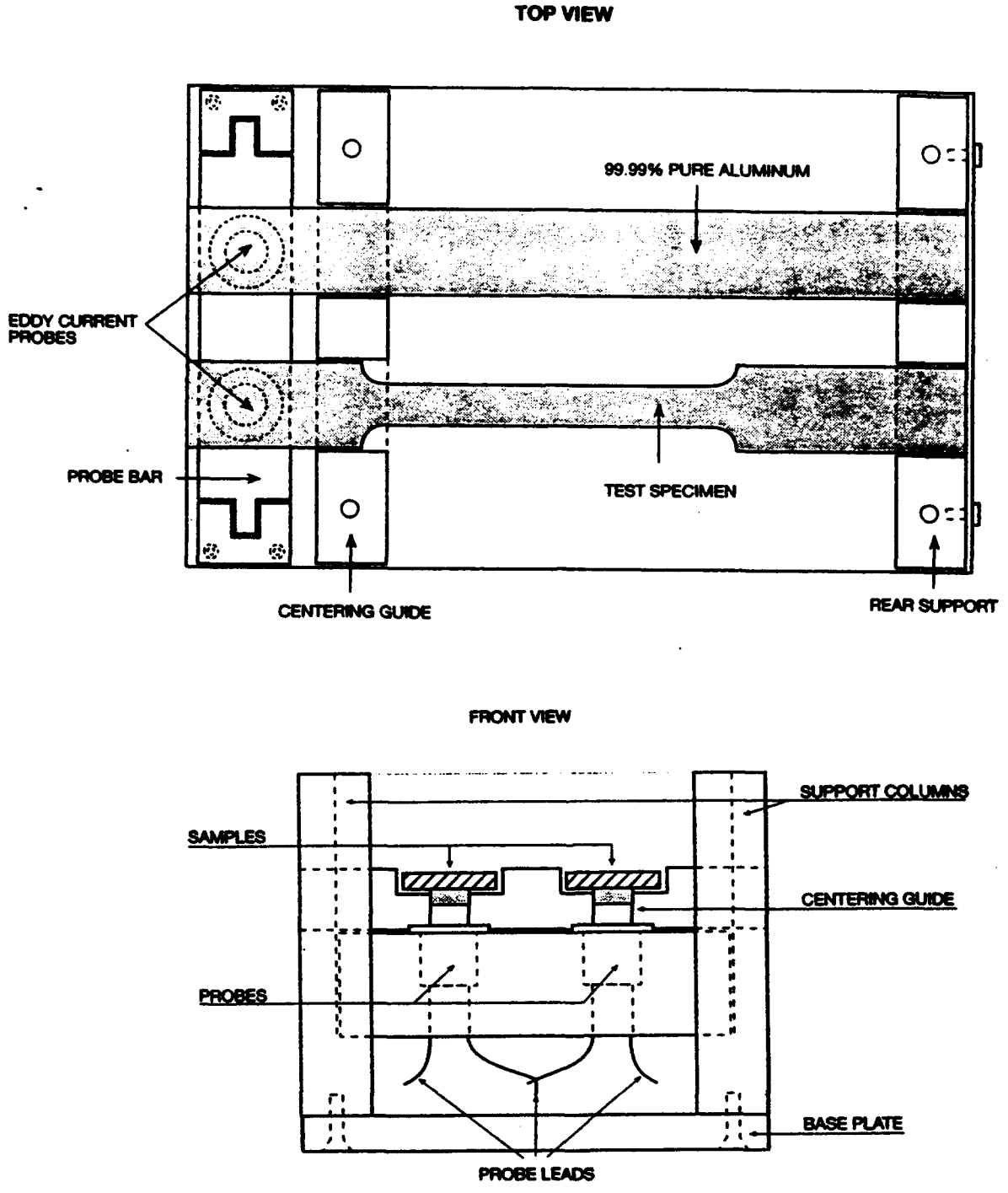

Figure 3.3 Schematic Drawings of Testing Apparatus.

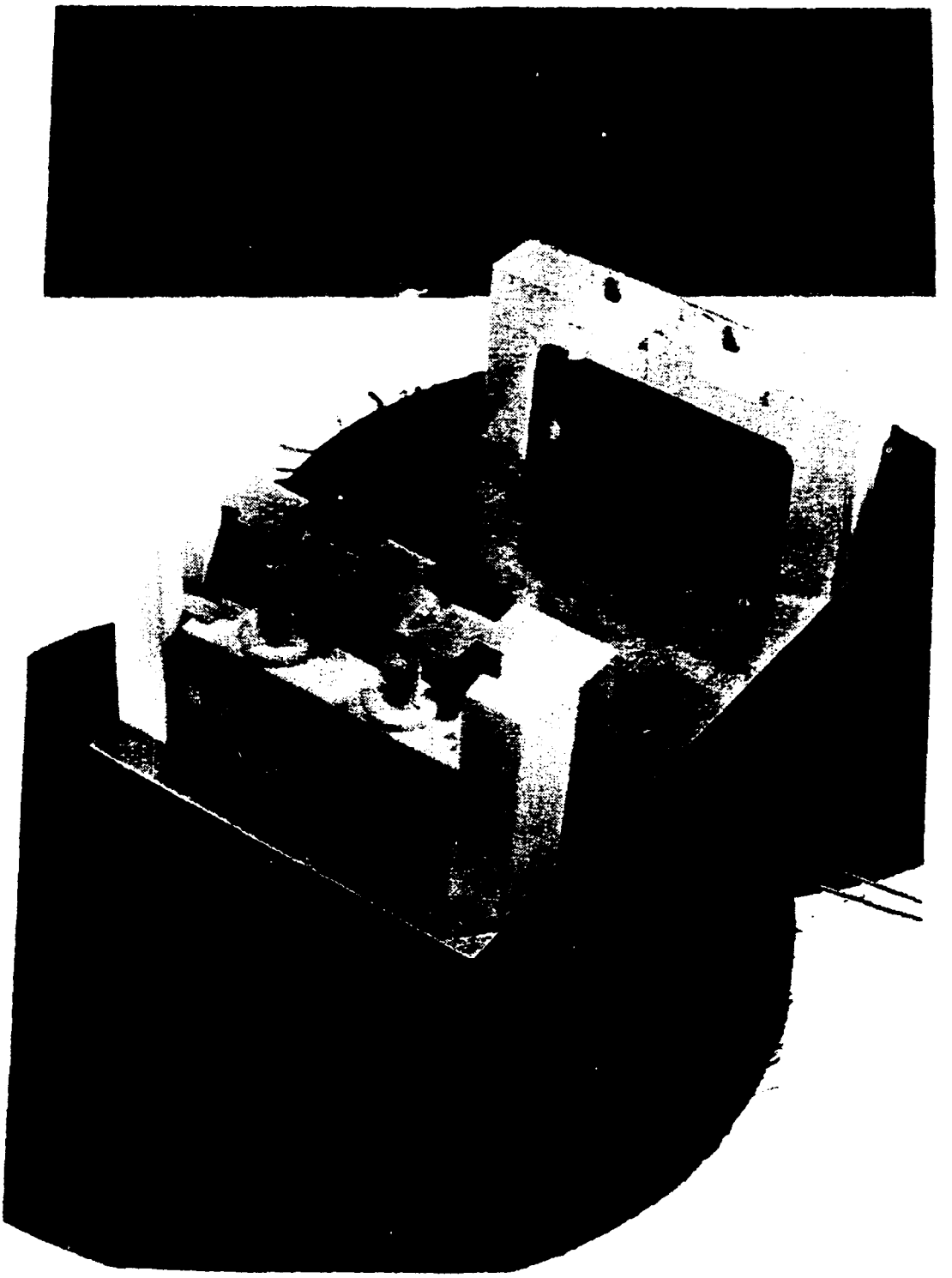

Figure 3.4 Photograph of Testing Apparatus and Test Probes.

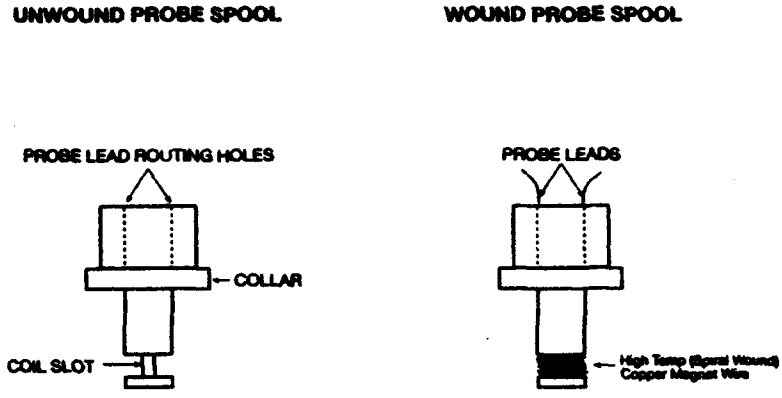

Figure 3.5 Schematic Drawing of Eddy Current Probe Coils

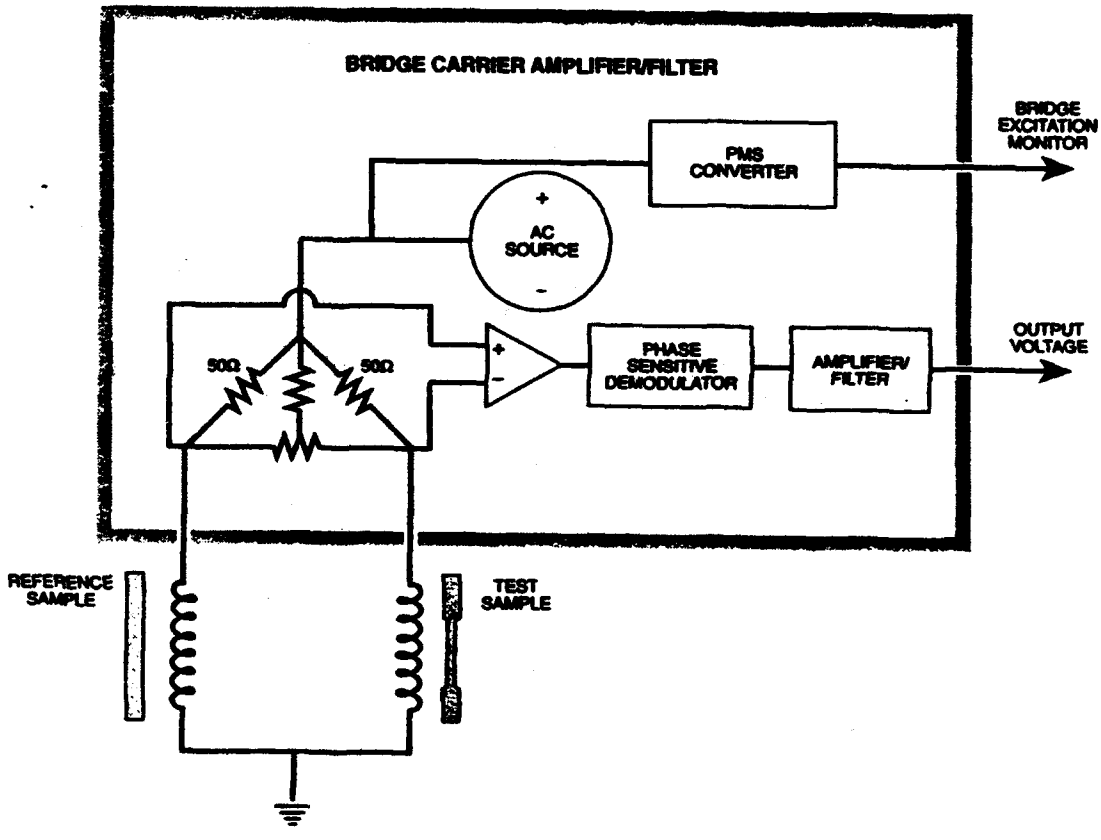

Figure 3.6 Block diagram of Bridge Carrier Amplifier/Filter

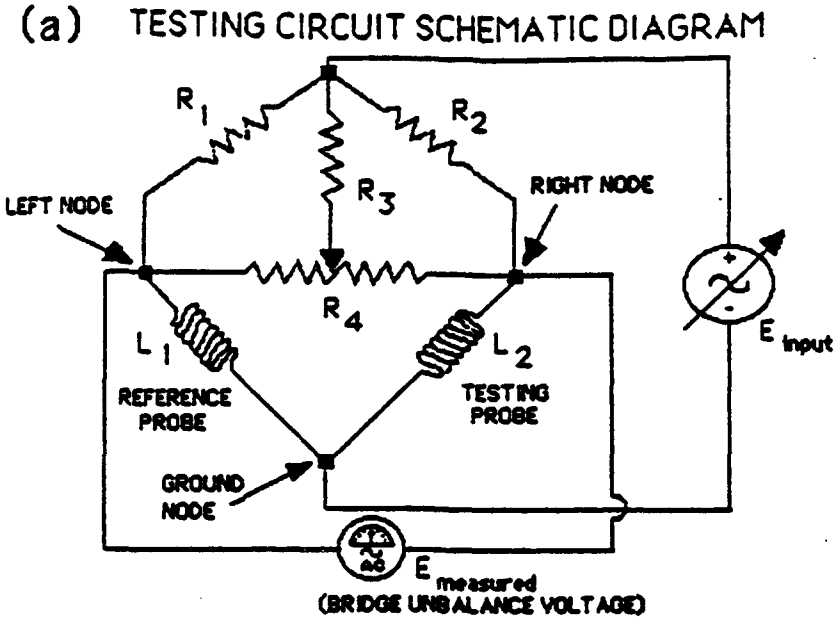

Figure 3.7 Simplified Impedance Bridge Circuit Drawing

D. MONITORING SYSTEM VALIDATION

A system validation was performed using the following steps:

(1) Two pure-aluminum samples were placed in the testing apparatus

(2) The furnace and samples were allowed to come to thermal equilibrium.

(3) A reference pure aluminum sample was taken out and allowed to cool to room temperature.

(4) Once the sample had cooled to room temperature, the data acquisition program was given sampling rate instructions and the sample was then reinserted into the furnace.

(5) The sample and furnace were allowed to reach thermal equilibrium once again.

The results are discussed in the next chapter.

IV. RESULTS AND DISCUSSION

A. Monitoring System Design and Operation

The eddy-current monitoring system was easy to operate but did experience some mechanical difficulties during the course of more than 60 testing cycles. Initially, the testing apparatus developed by Esarey was used in the monitoring system. Significant thermally induced embrittlement eventually required repair and modification of the testing apparatus. A repair to the test probe bar was made to minimize the distance between the probe support bar and the vertical support, which was thought to be made of Teflon®. The material actually used for this component had poorer heat resisting properties than expected of Teflon® and did not provide consistent probe and sample positioning especially at higher temperatures. The test probe support bar was eventually replaced by one fabricated of Teflon®. Following the replacement, the testing apparatus began to show signs of discoloration at temperatures above 180^0C which would have eventually led to thermally induced cracking. In order to avoid any cracking, testing was limited to a maximum temperature of 180^0C.

The new Bridge Carrier Amplifier/Filter (B.C.A.) did not present any problems during set-up and testing. The null

voltage was easily and repeatably adjusted to a value of approximately 0.00 V. However, the B.C.A. proved to be extremely sensitive to any relative movement of sample and eddy current probe and extra care had to taken to ensure that neither the sample nor any of the lead wires were disturbed during testing. Small disturbances could lead to a change in the output voltage value range. In addition, the Hewlett Packard multimeter, although self-calibrating, had a constant error of 3.502 mV. This error proved to be insignificant after the range of output voltage values were taken into consideration. Two electrical connections were initially soldered with a 60/40 lead-tin solder, they failed upon heating at 200^{0}C. As a result, the connections were restripped and resoldered with 95/5 tin-antimony solder for higher temperature testing. The newly soldered connections were covered by heat-resistant shrink tubing in an attempt to retard environmental degradation.

B. Bridge Carrier Amplifier/Filter Response

An equation for bridge output voltage (V_o) was reported by Esarey [Ref. 1] and is given by the relation:

$$V_o = \left[\frac{Z_1}{R_L + Z_1} - \frac{Z_2}{R_R + Z_2}\right] * V_i \qquad (4.1)$$

where Z_1 is the magnitude of the reference probe impedance, R_L is the resistance of the upper left bridge leg, Z_2 is the

magnitude of the testing probe impedance, and R_R is the resistance of the upper right bridge leg. The following conditions must be met in order to achieve a perfect null condition:

$$\frac{Z_1}{Z_2} = \frac{R_L}{R_R} \tag{4.2}$$

$$\frac{Z_1}{R_1} = \frac{Z_2}{R_R} \tag{4.3}$$

A perfect null was not necessary to satisfy the objective of this research project. However, the null unbalance voltage should be minimized within reasonable bounds, i.e. +/- 5mV. The actual values of the inductive bridge elements contained in equation 4.1 were measured under isothermal conditions for temperatures of either 120°C or 180°C with pure aluminum samples and using an impedance analyzer. The following equation was applied to the data:

$$Z_n = R_n + 2\pi fL \tag{4.4}$$

where R_n = DC resistance of coils and L = inductance of the coils. A nominal value of 50Ω was used for R_L and R_R. The resulting values for Z_1 and Z_2 are listed in Table 4.1.

TABLE 4.1 MEASURED BRIDGE ELEMENT VALUES (Taken from Esarey, 1992)

Temp. (°C)	Z_1 (Ω)	Z_2 (Ω)
120	20.427	19.937
200	21.054	20.447

C. Experimental Measurements For Pure Aluminum

The procedure discussed in Chapter III was used to perform initial testing with the pure aluminum samples. Based on electromagnetic and physical principles discussed in Chapter II, theoretical bridge output versus time curves were plotted as shown in Figure 4.1. The increase in resistivity changes the impedances of the eddy current coils. Because pure aluminum is being used with both coils the, theoretical bridge-output versus time curves should return to the initial null voltage (0.00V) upon re-attaining thermal equilibrium. The measured characteristics for pure aluminum are shown in Figure 4.2. The response from 0 to 10 seconds is a transient in which the coil is quenched by the room temperature sample. The response after approximately 10 seconds clearly is very similar to that of the predicted bridge output. The plot also demonstrates that fully annealed pure aluminum does not exhibit any changes in resistivity under isothermal conditions. The constant voltage under isothermal conditions is consistent with the non-aging response of pure aluminum. Lastly, the data indicated that the sample reached thermal equilibrium after approximately 1000 seconds.

It should be noted that voltage values obtained for higher testing temperatures, e.g. 160°C, are always lower than those at lower temperatures, e.g. 120°C. The explanation for the decreased voltage output values is two-fold. First, as

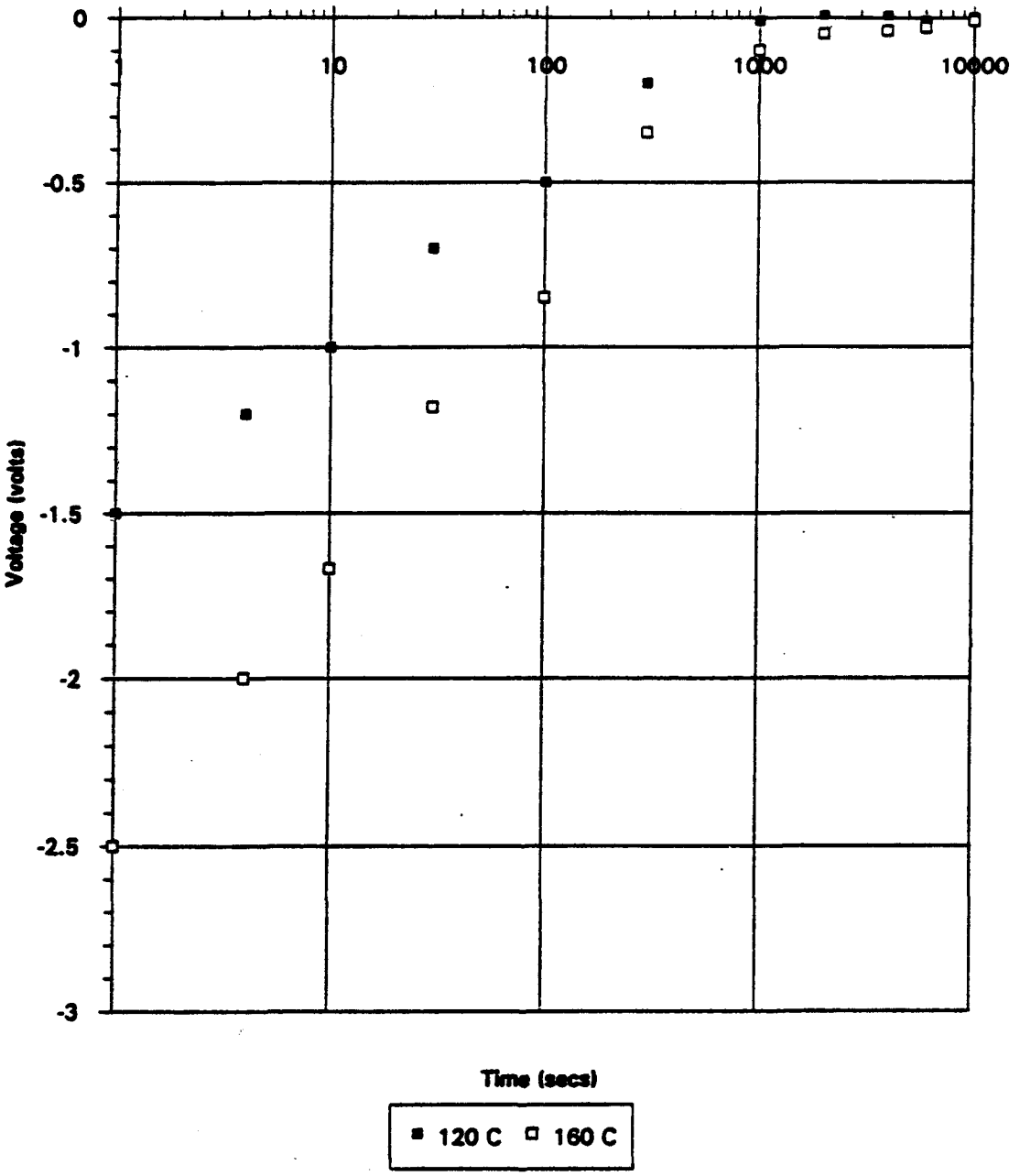

Figure 4.1 Theoretical Bridge Output Response Using for Pure Aluminum.

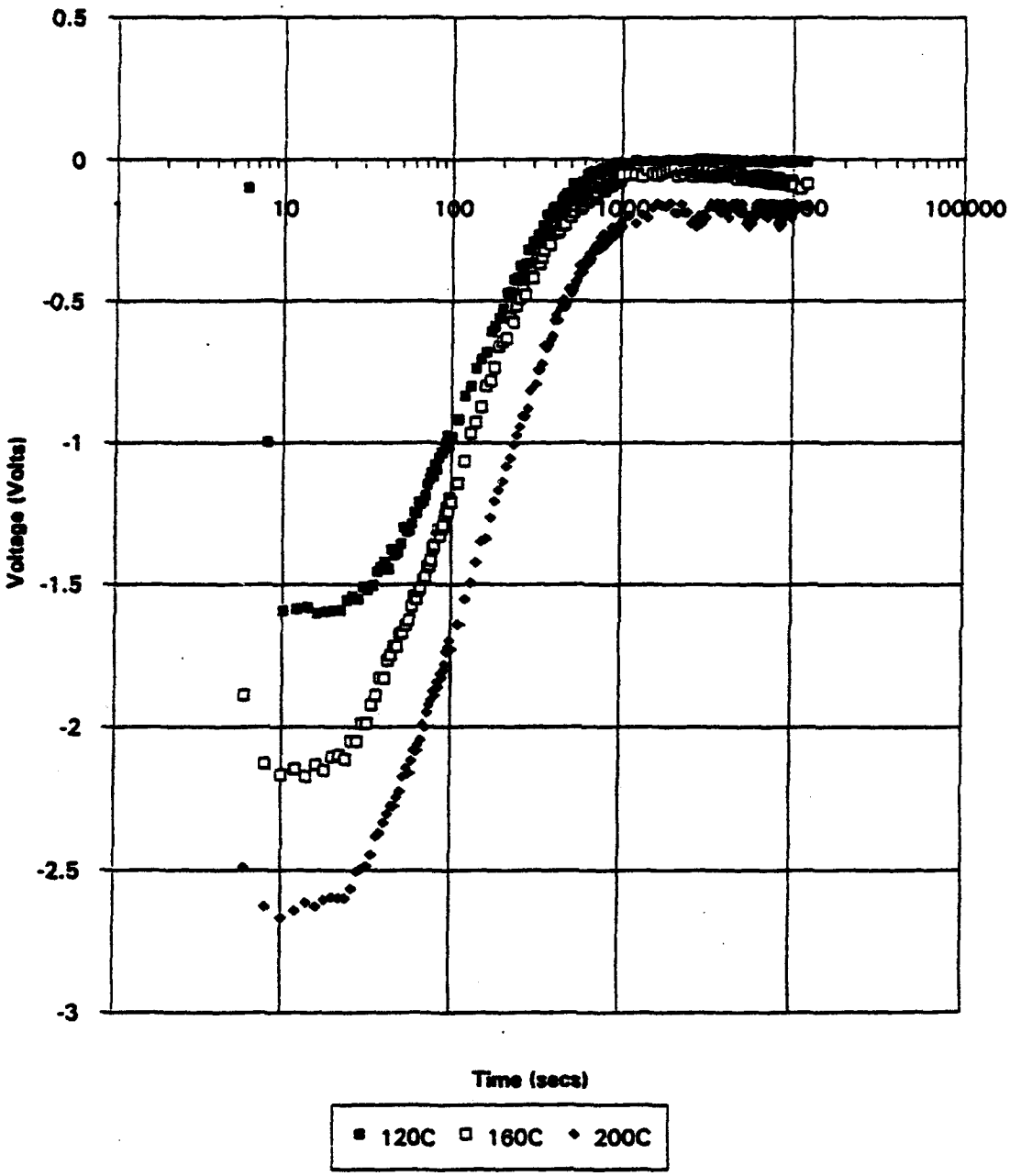

Figure 4.2 Experimental Bridge Output Response (Pure Aluminum Samples)

temperature is increased, the resistances within the eddy current coil windings as well as the reference sample increase. This increase in resistivity lowers the magnitude of the alternating current flowing through the coils since they are operated with a constant-voltage excitation source. e reduced flow of current then reduces the magnetic field generated. The reduced magnetic field, in turn, reduces the magnitude of the induced eddy currents within the sample, which reduces the inductive reactance of the coils. Therefore, the change of inductance reactance of the reference coil varies with an increase of temperature which in turn varies the initial bridge output value.

The second cause for the decrease of output voltage as temperature is increased is the difference in reference samples. The two pure aluminum reference samples were thought to be 99.99% pure aluminum. However, it became apparent that the samples were not identical. A simple two-part experiment was conducted to verify this:

(1) Both samples were placed in the testing apparatus and allowed to reach thermal equilibrium.

(2) The furnace temperature was raised to a higher temperature.

If both samples were the same, the output voltage should have remained at the null voltage. This was not the case, as shown in Figure 4.3. The samples were then removed and the heating

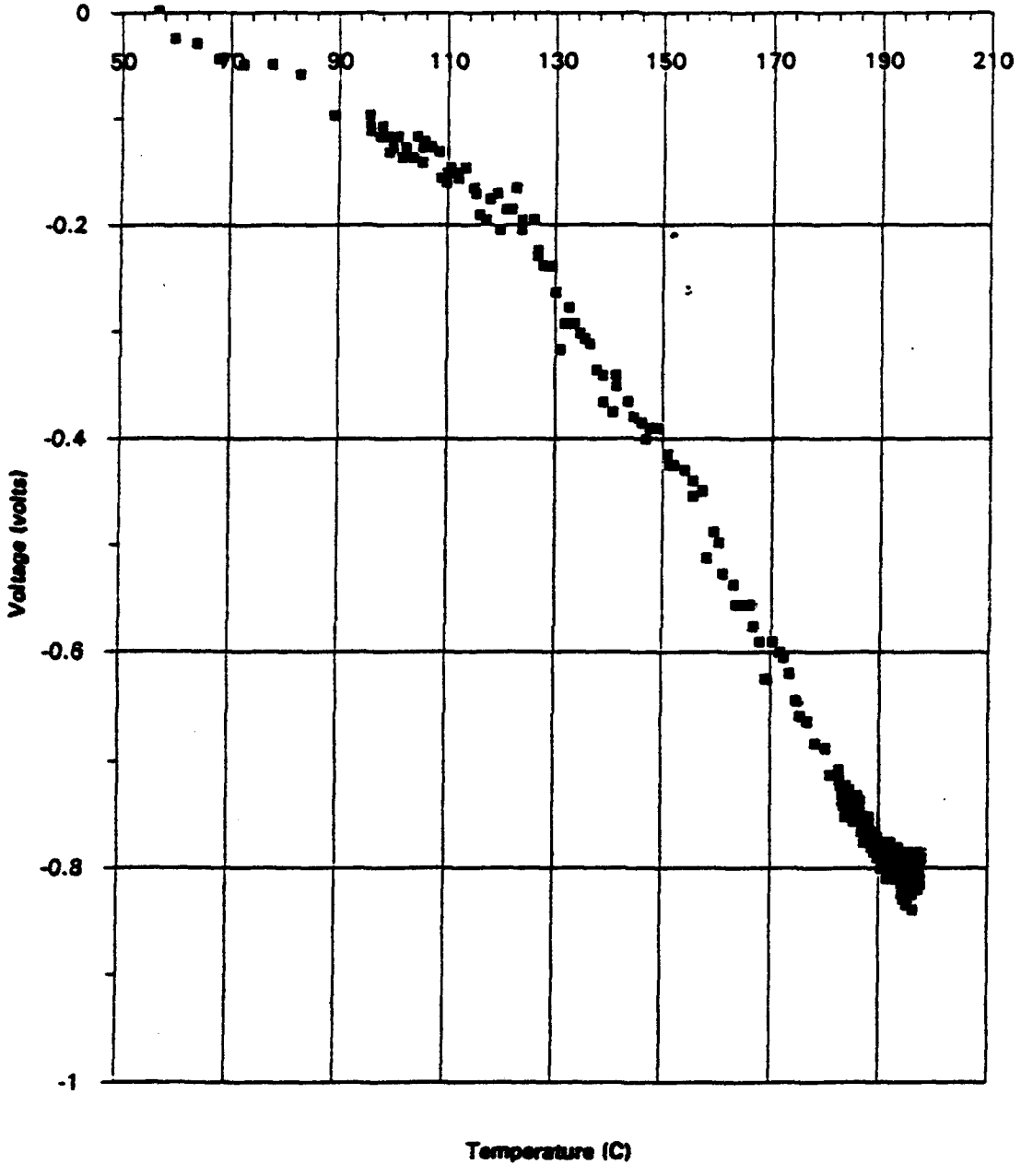

Figure 4.3 Apparent Output Voltage Drift

experiment was conducted with only the coils. The output voltage remained at the initial null voltage throughout the increase of temperature, as expected. It was then concluded the two samples had slightly different resistivities.

D. Experimental Measurement Results for Al 7075 Alloy

The voltage versus time curves in Figure 4.4 illustrate the bridge response characteristics as ANSI 7075 aluminum samples were aged for various temperatures. The bridge output characteristics were very similar to those obtained by Esarey with the exception of the much larger output voltage values in this work. The higher overall output values were a result of the amplifier within the B.C.A.

For each test temperature, a characteristic and continuous increase in bridge output values was seen in the process of reaching thermal equilibrium. Also, the rate of increase was temperature dependent. This initial increase in output voltage may reflect an increase in resistivity of the Al 7075 sample due to the formation of GP zones in the early stages of aging. The formation of GP zones is a nucleation and growth process and, for the aging temperature of interest here, their rate of increase is expected to increase with the increasing temperature. This is summarized in Figure 3.10 and 3.11 from Mondolfo [Ref. 12]. These data, for an alloy of 6.5% Zn and 2.5% Mg (near to the composition of Al 7075), indicate that GP

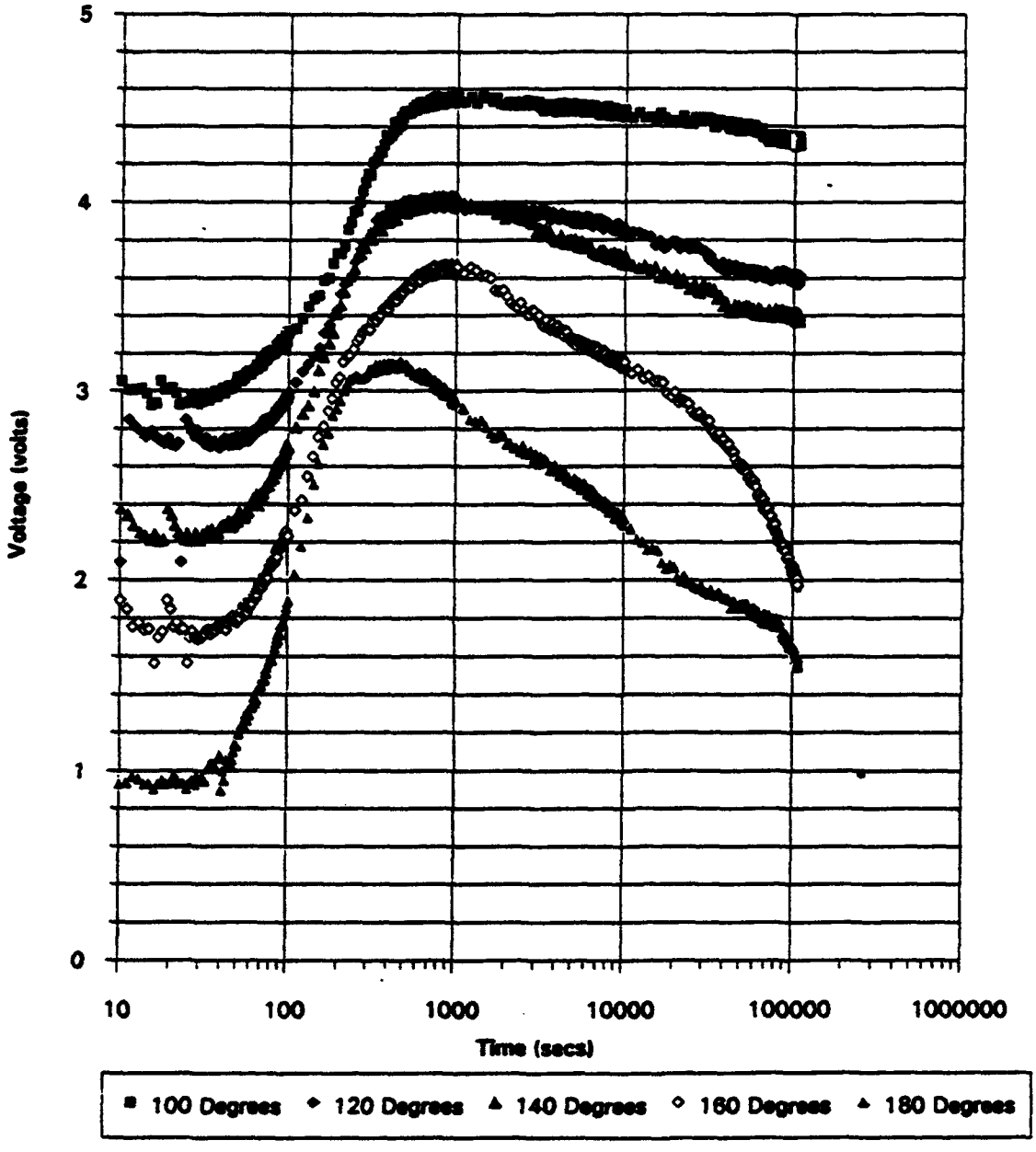

Figure 4.4 Experimental Bridge Output Response for Al 7075 Data Aged at Various Temperatures

zone formation will begin at times between 100 and 300s ($\sim 10^{-2}$-10^{-1}hr) for isothermal aging at temperatures up to 475K (200°C). From this, initial formation of GP zones is expected to coincide with initial heating and stabilization during testing.

Also, the peak voltage values decrease and are reached sooner as temperature is increased. The decrease in peak voltage is for the reason as was the case for the pure aluminum. The more rapid formation of the GP zones and transition to the η'-phase (curve B) is the reason for the greater rate of decrease in voltage values as temperature increases.

At higher temperatures (180^0 C and greater), the intermediate precipitates form after only a very short aging time. The rate of decrease of output voltage increases as the formation of the η' precipitates increases. As the rate of precipitation is accelerated, zinc and magnesium solutes (which act as scatterers of electrons) precipitate from the aluminum matrix at an accelerated rate. The larger η' precipitates differ from the smaller GP zones not only in size but also scatter electrons to a lesser degree, thus, the resistivity decreases faster with increased aging temperature and times. This is shown in Figure 4.4.

E. Mechanical Testing

In order to reach the desired objective of correlating bridge output values with mechanical test data, a series of mechanical tests were conducted on room temperature test samples age 120^0C for various aging times. The bridge output voltage values were superimposed on one another and these are presented in Figure 4.5. Individual tests are presented in Appendix A. Samples were stored at -15^0C to prevent any natural aging from

occurring while awaiting further testing. Hardness, yield, ductility and ultimate strength test results are presented in Figure 4.6. The mechanical test results correlated with bridge output values could serve as the design basis for a control device/apparatus used to monitor the age hardening of aluminum alloys and other metals.

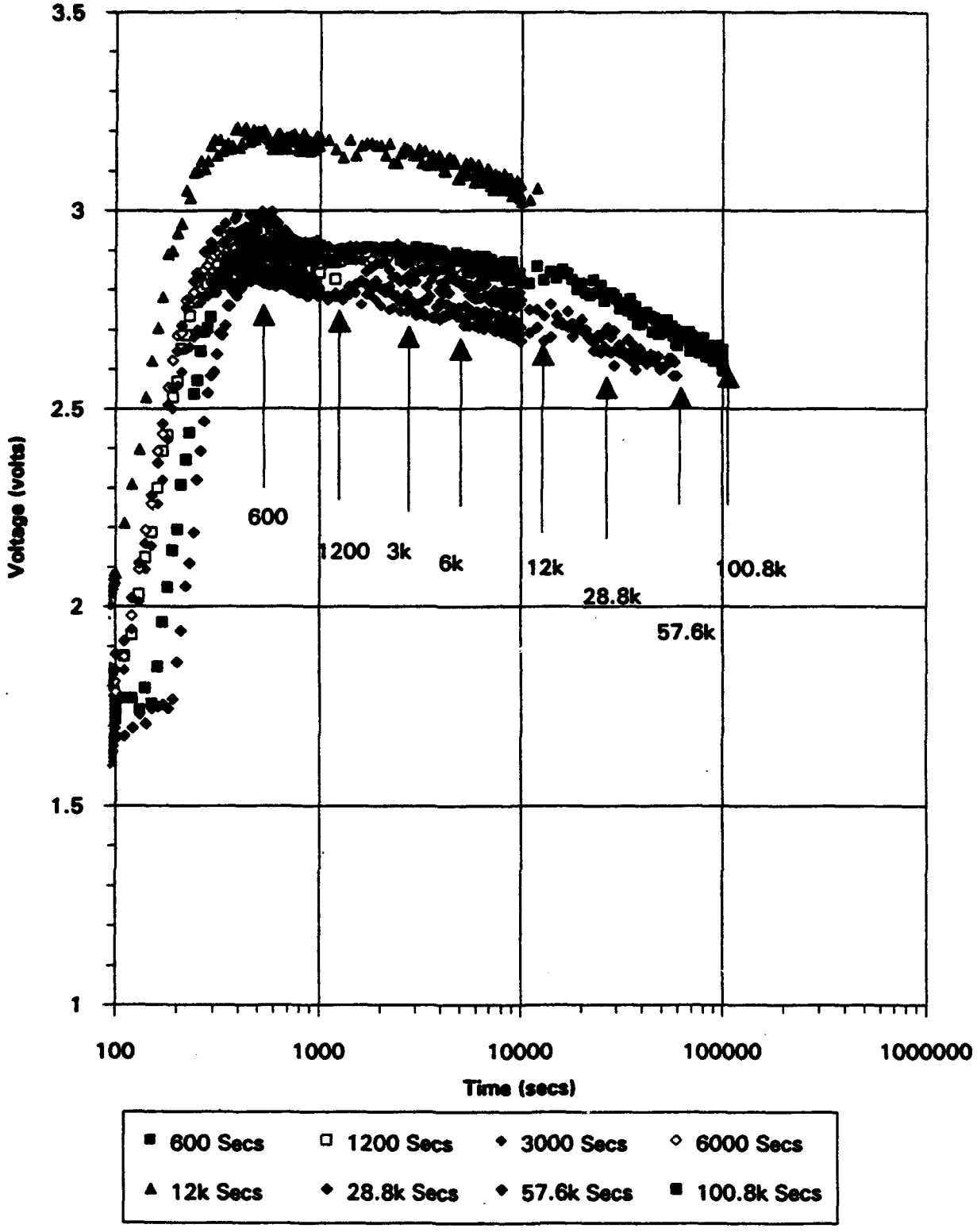

Figure 4.5 Al 7075 Aged at 120°C for Various Times.

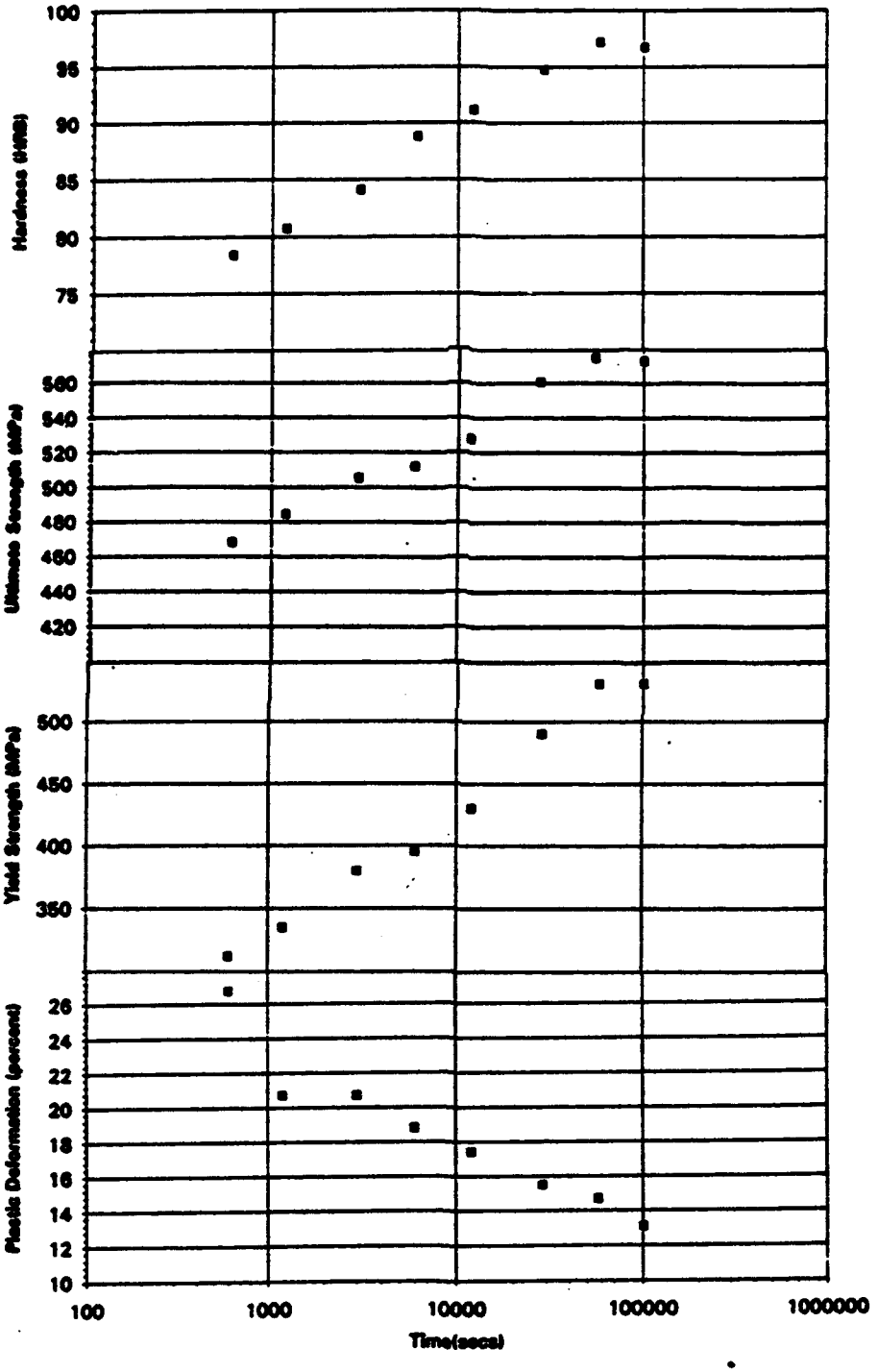

Figure 4.6 Experimental Al 7075 Mechanical Test Results

V. CONCLUSIONS AND RECOMMENDATIONS

The conclusions and recommendations discussed below were drawn as a result of this thesis project.

A. CONCLUSIONS

1. Testing Apparatus Design

The functional aspects of the testing apparatus were sound and need not be modified to perform further testing. Consistent sample and coil positioning can now be achieved. However, the entire testing apparatus should be remanufactured from a more heat resistant material for higher temperature testing (see recommendations).

2. Bridge Carrier Amplifier/Filter

The phase sensitive demodulator greatly simplified the nulling process. It allowed the null voltage to be lowered to and through 0.00 volts. The amplifier/filter allowed easy adjustment of output voltage values to a more usable voltage range of +/- 10 volts.

3. Monitoring Concept

The monitoring concept was determined to be valid as verified by the pure aluminum sample results of return to the minimum null voltage and the infinite resistance (air) sample results. Also, the rate of increase and decrease in final

output values increased with an increase in aging temperature which is consistent with the known aging response of Al 7075.

B. RECOMMENDATIONS

The entire testing apparatus should be reconstructed from a glass ceramic material such as MACOR® by DuPont and the coils should be professionally wound with platinum wiring. This would allow continuous testing up to 800°C necessary for higher strength alloys such as titanium alloys. The professional winding of coils would reduce the difference of inductive reactance between the two coils and thus increase the accuracy of the testing system.

Further mechanical testing of aluminum alloy sample aged at various temperatures needs to be conducted to further unlock the potential of such a system in the monitoring the age hardening of aluminum alloys.

The excitation voltage of approximately 5 Vrms and 52Khz was used to maximize depth of penetration. Further testing is required to optimize the balance between test frequency, probe size, and depth of penetration.

APPENDIX A: EXPERIMENTAL BRIDGE OUTPUT VALUE VS TIME GRAPHS

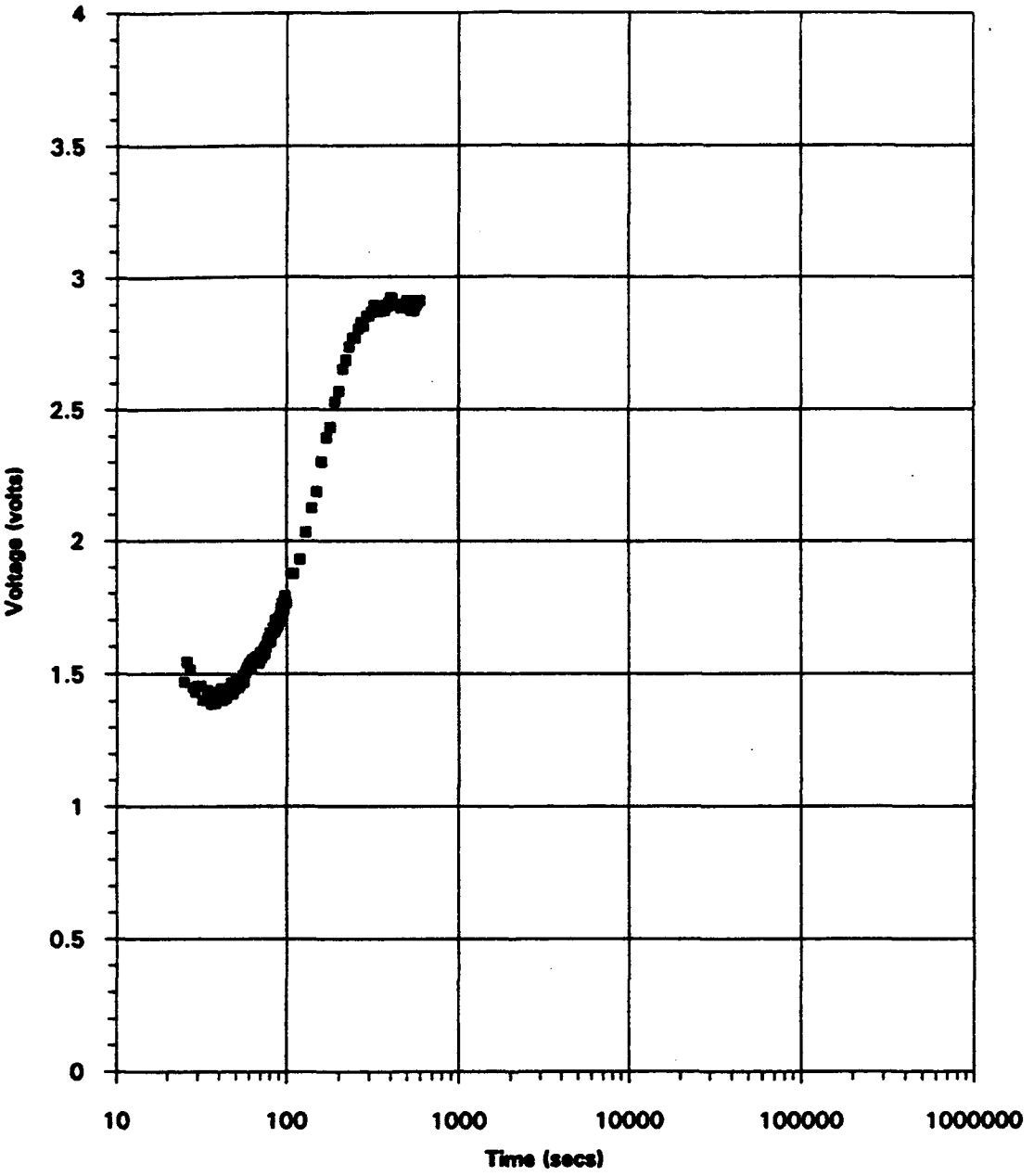

Figure A.1 Experimental Bridge Output Values for Al 7075 Aged at 120^{0}C for 600 Seconds

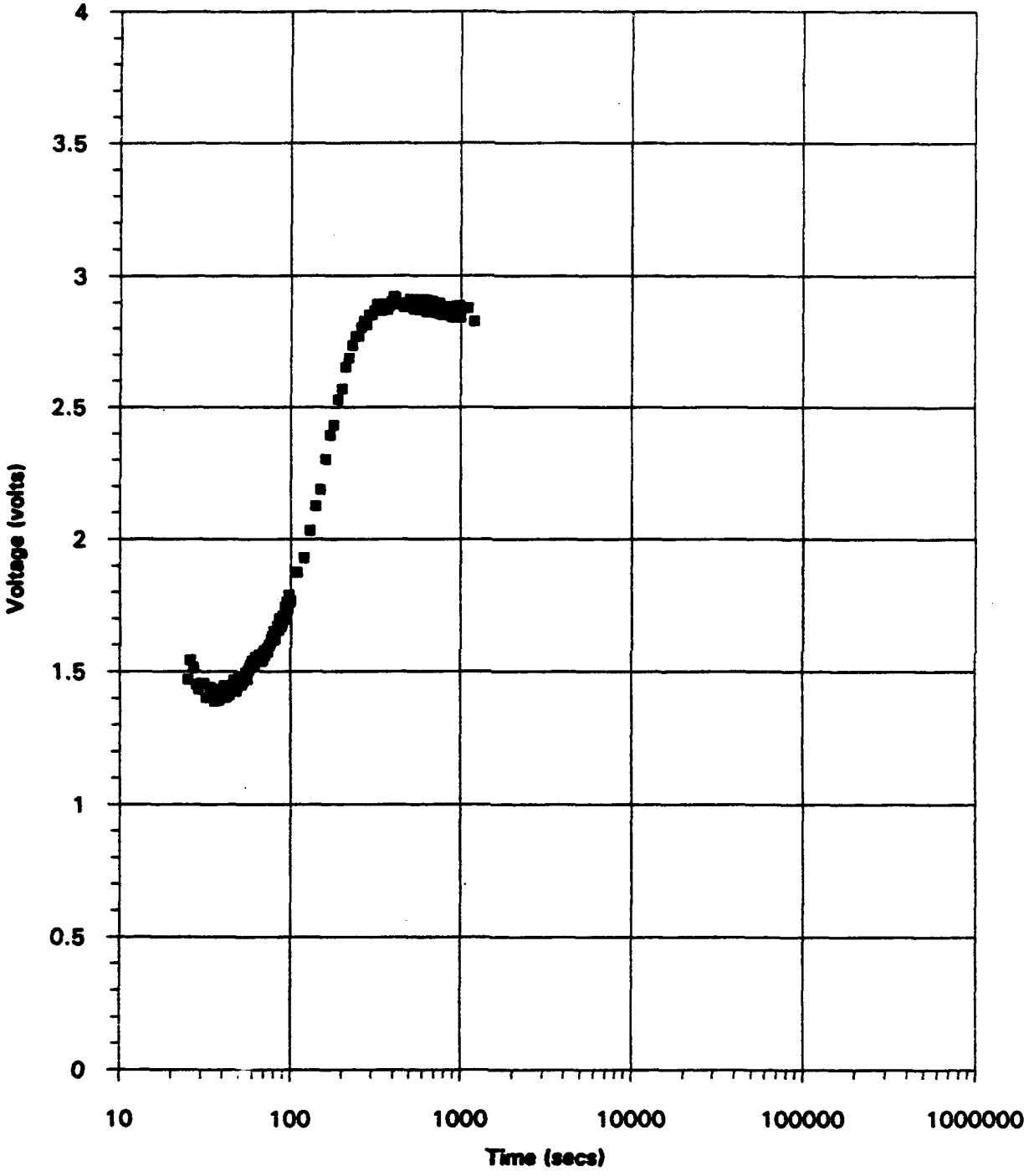

Figure A.2 Experimental Bridge Output Values for Al 7075 Aged at 120^{0}C for 1200 Seconds

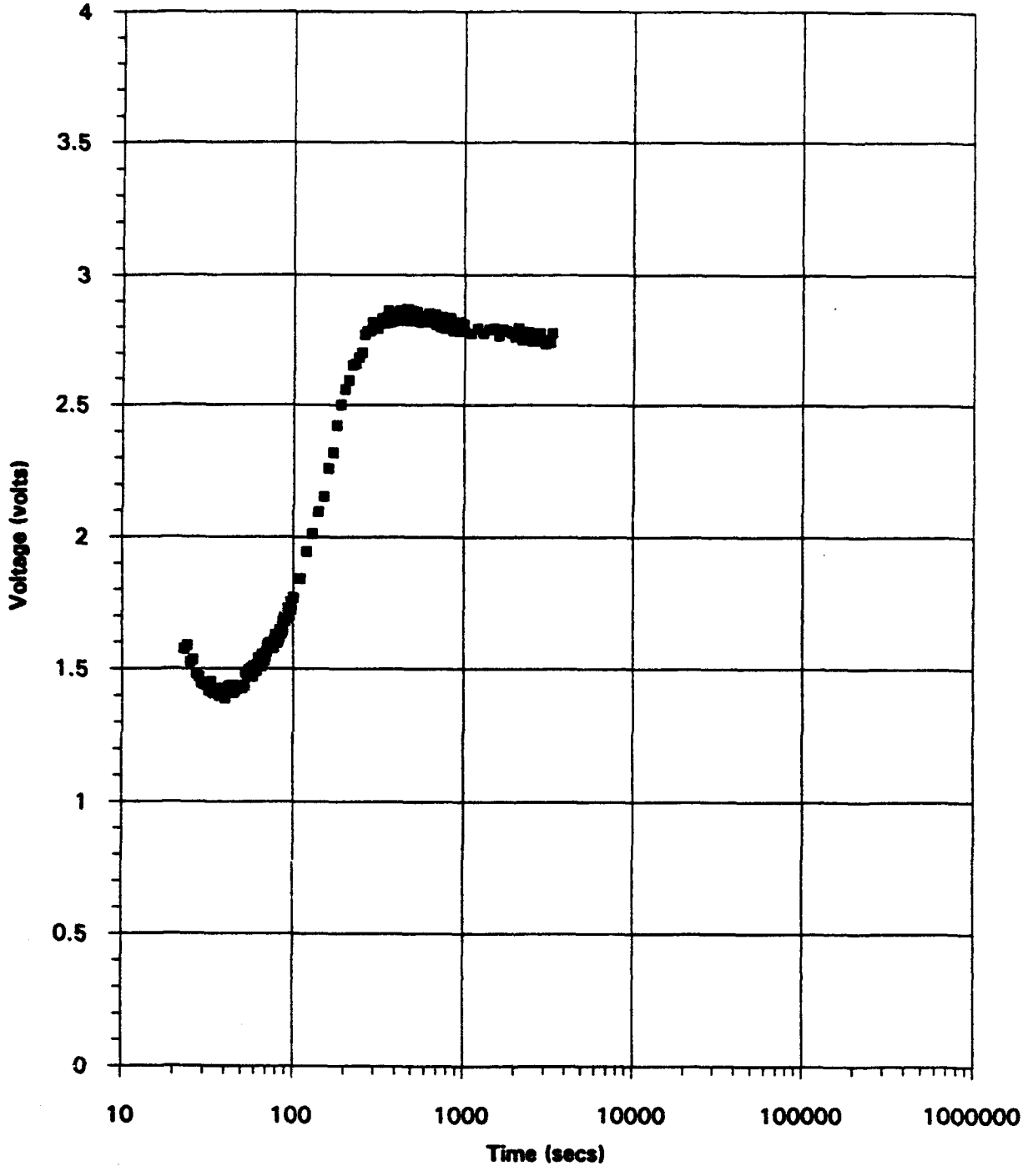

Figure A.3 Experimental Bridge Output Values for Al 7075 Aged at 120^{0}C for 3000 Seconds

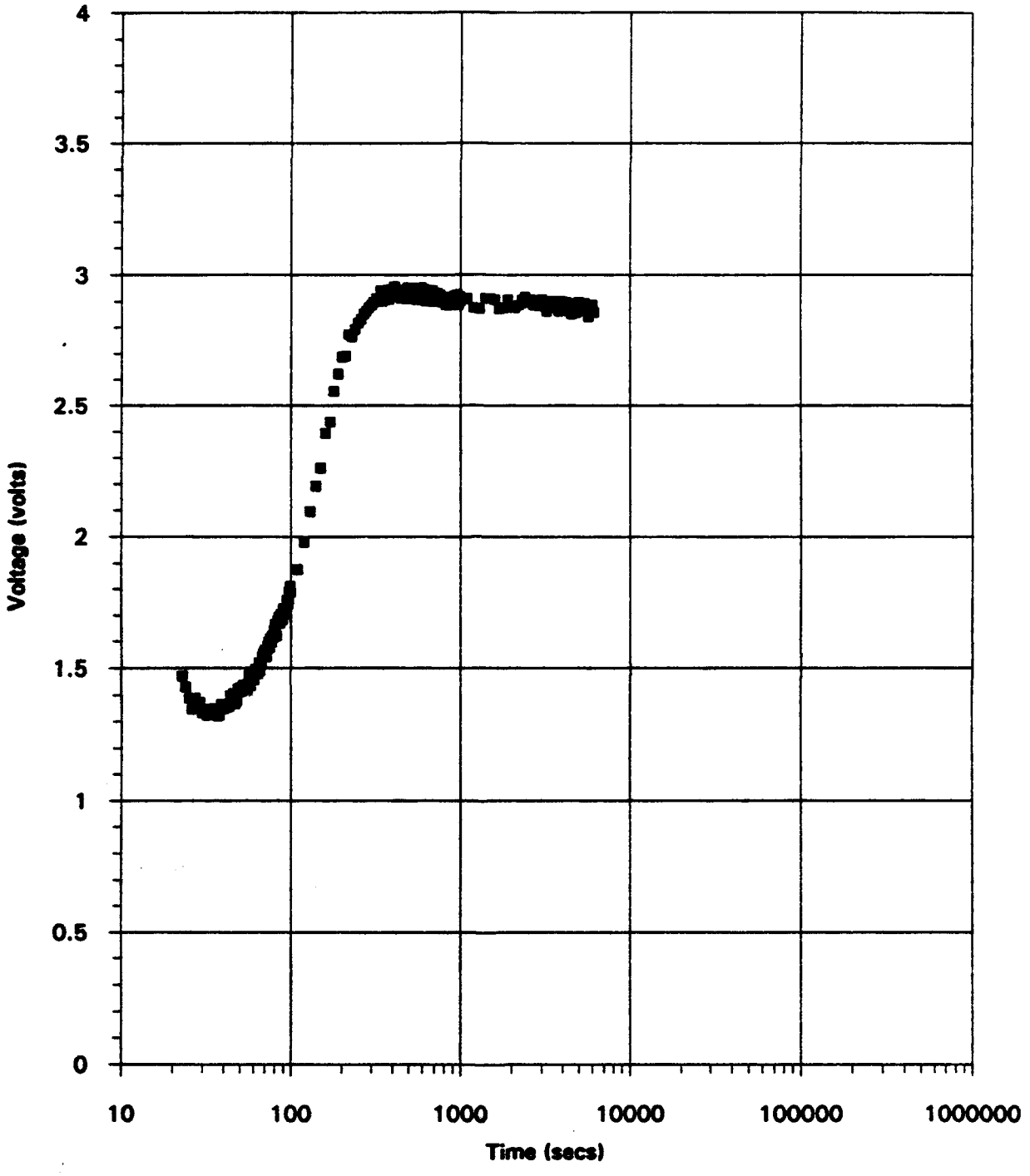

Figure A.4 Experimental Bridge Output Values for Al 7075 Aged at 120^{0}C for 6000 Seconds

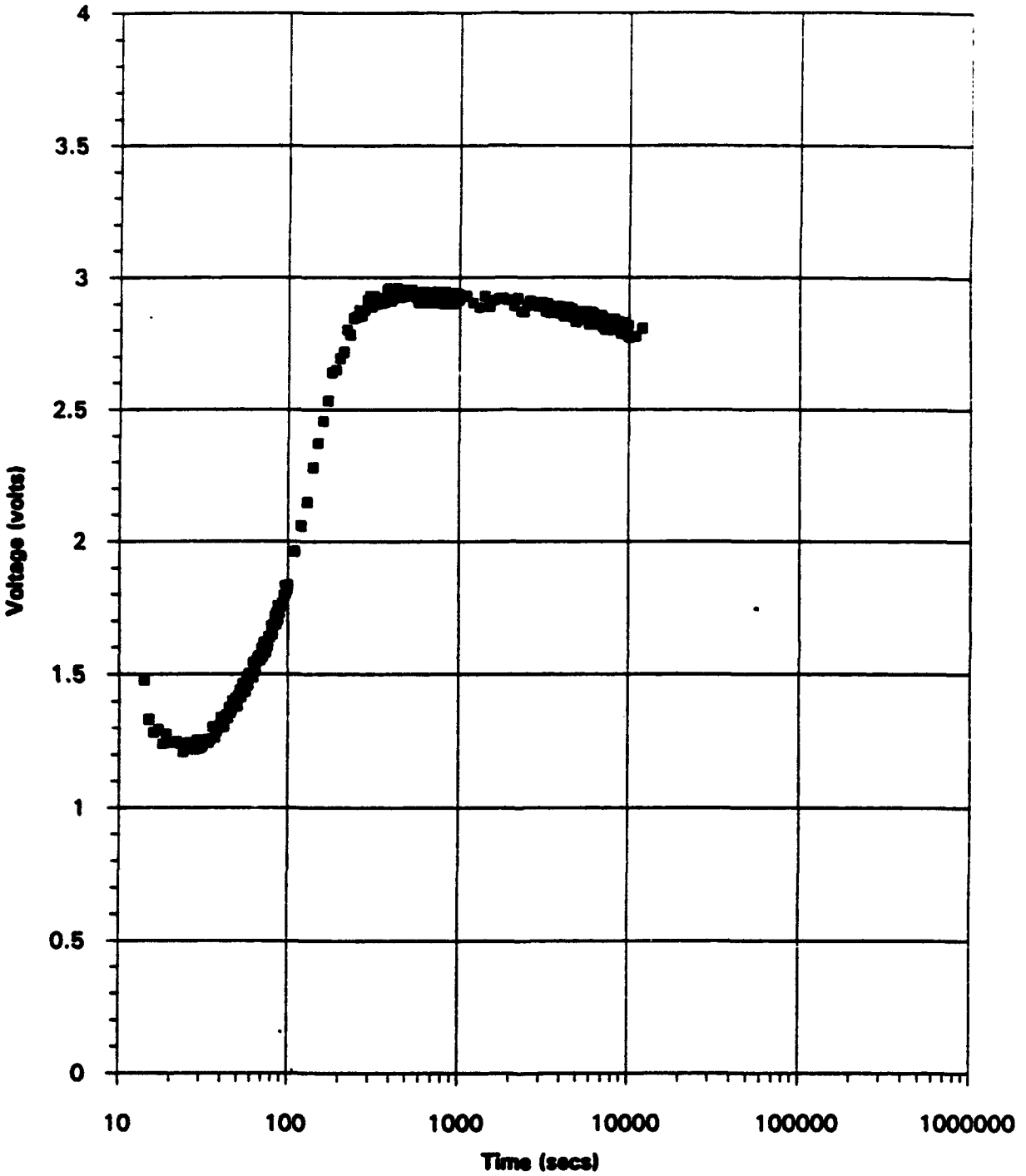

Figure A.5 Experimental Bridge Output Values for Al 7075 Aged at 120^0C for 12000 Seconds

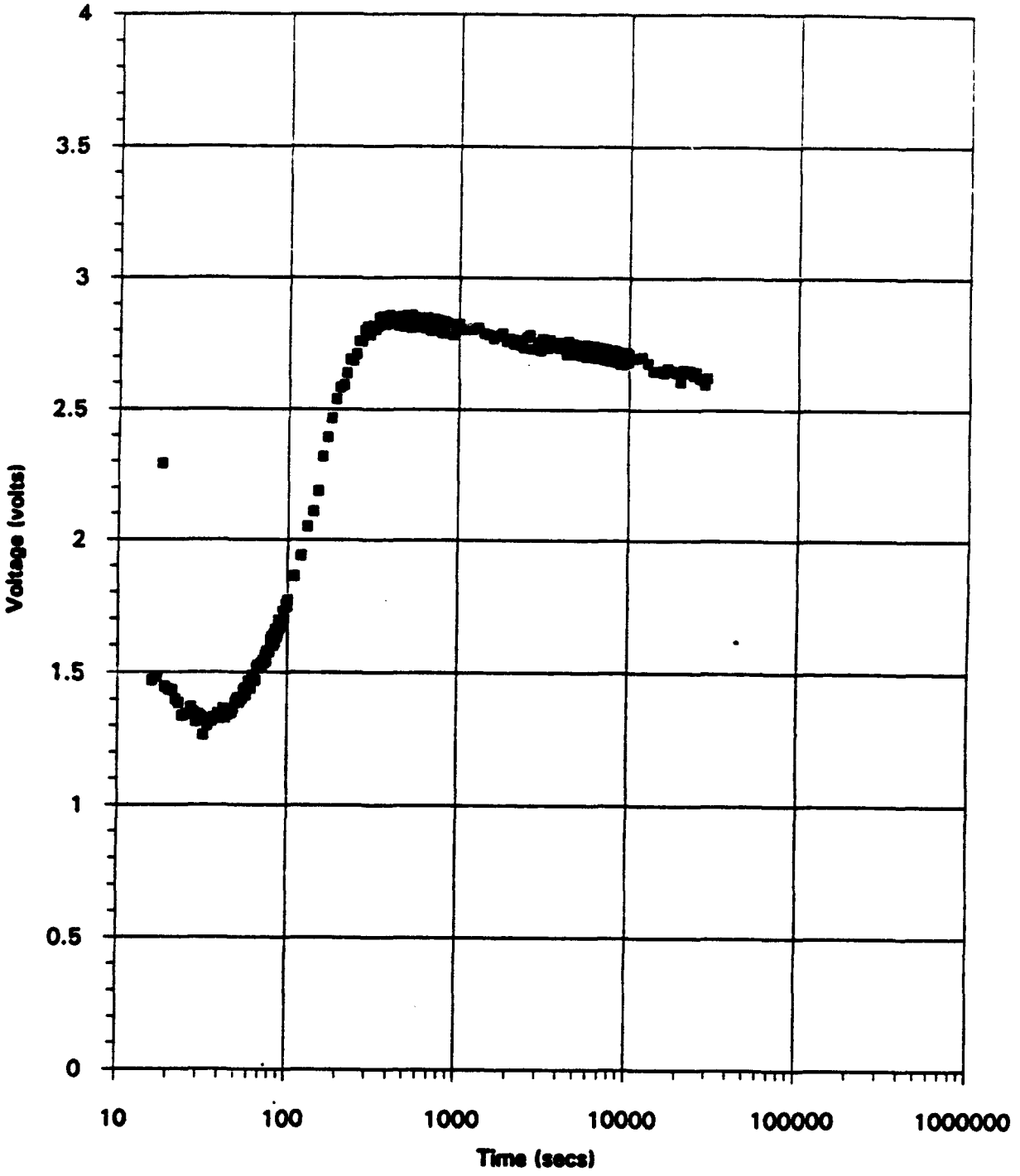

Figure A.6 Experimental Bridge Output Values for Al 7075 Aged at 120^{0}C for 28800 Seconds (8 hrs)

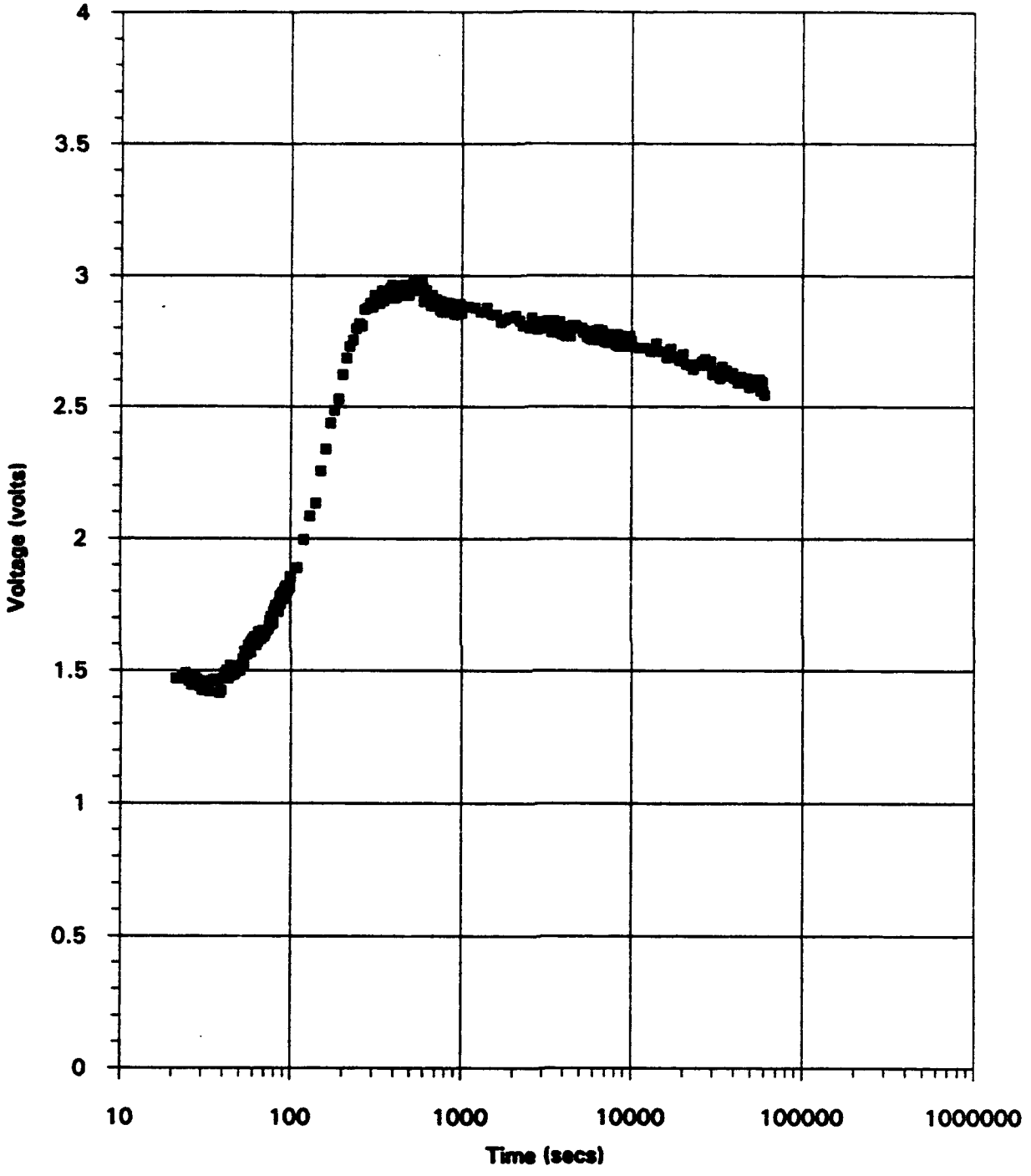

Figure A.7 Experimental Bridge Output Values for Al 7075 Aged at 120^{0}C for 16 Hours

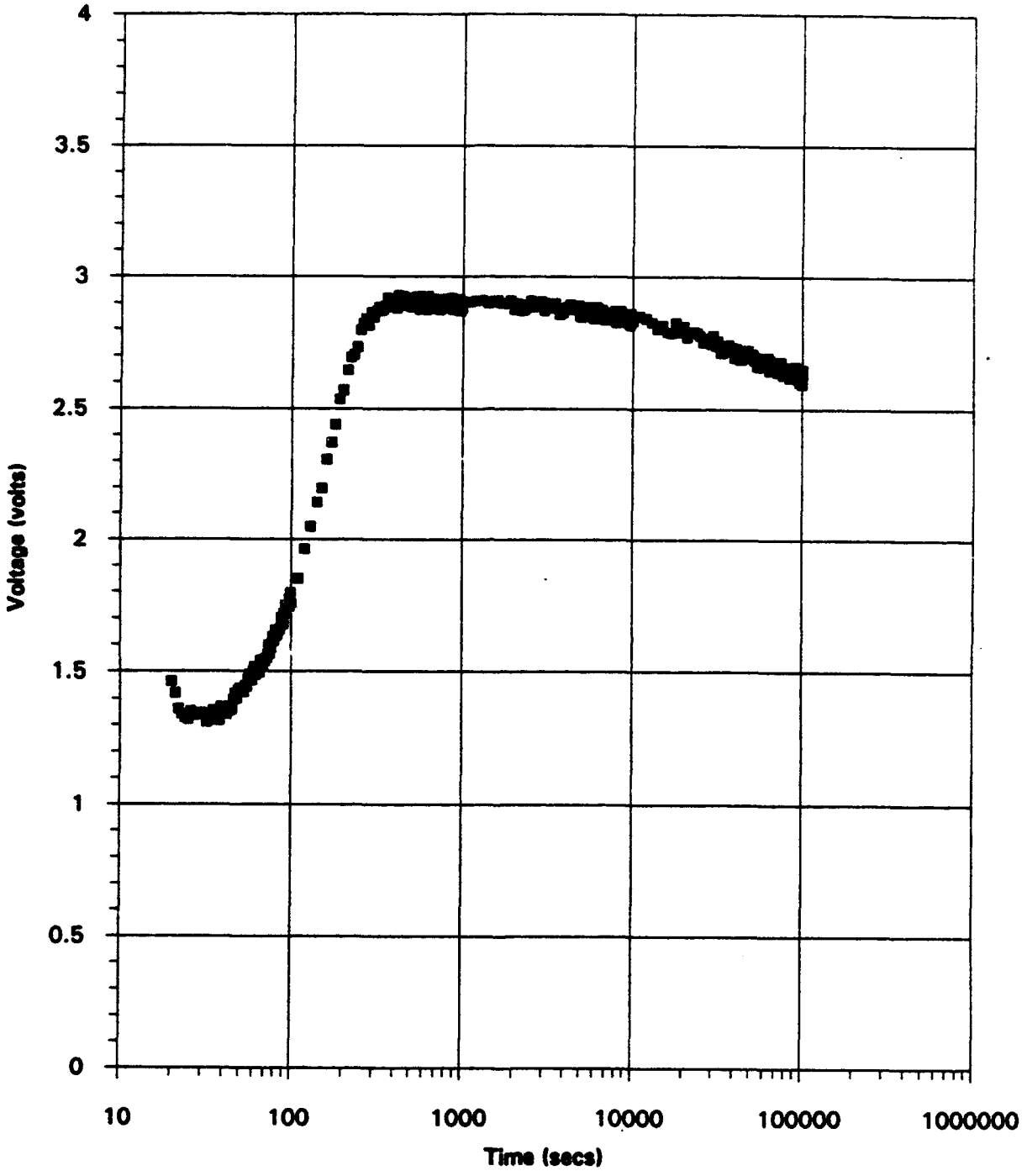

Figure A.8 Experimental Bridge Output Values for Al 7075 Aged at 120^{0}C for 28 Hours

LIST OF REFERENCES

1. Esarey, John G., *Continuous Measurement By Eddy Current Methods of Age Hardening in Aluminum Alloys,* Master's Thesis, Naval Postgraduate School, Monterey, California, September, 1992.

2. *Metals Handbook,* 10th Edition, v.17, pp.164-194, American Society for Metals, 1990.

3. Metal Handbook, 10th Edition, v.2, pp.115-116, American Society for Metals, 1990.

4. Askeland, Donald R., *The Science and Engineering of Materials,* PWS-KENT Publishing Co., 1989.

5. Callister, D.R., *Material Science and Engineering, An Introduction,* John Wiley & Sons, Inc., 1991.

6. National Aeronautics and Space Administration Report 5113 (NASA SP-5113), *Nondestructive Testing: A Survey,* pp.101-117, 1973.

7. McGonnage, Warren J., *Nondestructive Testing,* pp. 346-390, Gordon and Breach, 1969.

8. Rosen, M., "Eddy Current Analysis of Precipitation Kinetics in Aluminum Alloys," *Metallurgical Transactions A,* v.20A, pp. 605-610, April 1989.

9. Rosen, M., Horowitz, E., Swartzendruber, L., Fink, S., Mehrabian, R., "The Aging Process in Aluminum 2024 Studied by Means of Eddy Currents," *Materials Science and Engineering,* v.53, pp. 191-198.

10. Seltzer, David D., *Correlation of Conductivity to Mechanical Properties of Age-Hardenable Aluminum Alloys Using Eddy Current Methods,* Paper from the "Proceddings for the Fifth International Conference on Nondestructive Testing", Department of Energy, Nines and Resources, 1969.

11. Rummel, W.D., *Characterization of 2014,2219, 6061 and 7075 Aluminum alloy Heat Treatment Response by Eddy Current Conductivity, Hardness and Mechanical Properties,* American Society for Nondestructive Testing, Inc., 1980.

12. Porter, D.A., Easterling, K.E., *Phase Transformations in Metals and alloys,* Van Nostrand Rheinhold Co. Ltd., 1981.

13. Smallman, R.E., *Modern Physical Metallurgy,* Butterworths, 1985.

14. Hatch, John E., *Aluminum, Properties and Physical Metallurgy,* American Society for Metals, 1984.

15. Embury, J.D., "Electron-Microscopic Studies of Precipitation in Aluminum Alloys", *Journal of the Institute of Metals,* v. 87, pp.429-438, 1989.

16. Mondolfo, L.F., *Aluminum Alloys, Stuctures and Properties,* Butterworths, 1976.

17. Private communication between Tom Christian, Electonic Instrument Support, Code 34 and Silvester Mata, 04 October, 1993.

INITIAL DISTRIBUTION LIST

1.	Defense Technical Information Center Cameron Station Alexandria, Virginia 22304-6145	2
2.	Library, Code 52 Naval Postgraduate School Monterey, CA 93943-5002	2
3.	Chairman, Code ME Department of Mechanical Engineering Naval Postgraduate School Monterey, CA 93943-5000	1
4.	Dr. Terry R. McNelley, Code ME/MC Department of Mechanical Engineering Naval Postgraduate School Monterey, CA 93943-5000	2
5.	Dr. William Frazer, Code 6063 Naval Air Warfare Center Warminster, PA 18974	2
6.	Silvester G. Mata c/o Maria G. Mata 4802 South 10th Street Phoenix, AZ 85040	1